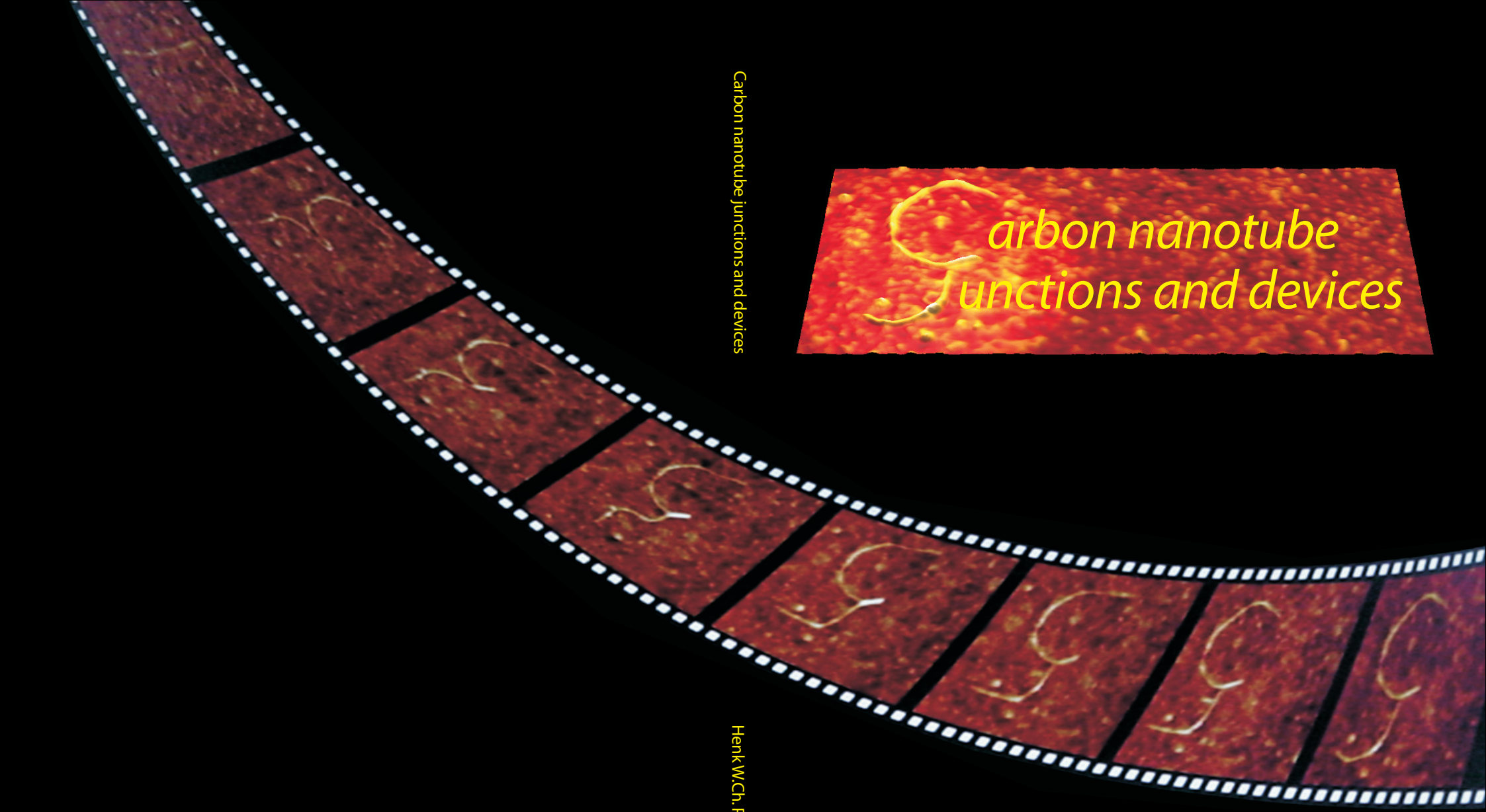

Carbon nanotube junctions and devices

Henk W.Ch. Postma

ISBN 90-704-2258-7

DUP Science

Carbon nanotube junctions and devices

Carbon nanotube junctions and devices

Proefschrift

ter verkrijging van de graad van doctor
aan de Technische Universiteit Delft,
op gezag van de Rector Magnificus prof.ir. K.F. Wakker,
voorzitter van het College voor Promoties,
in het openbaar te verdedigen op dinsdag 4 december 2001 om 10.30 uur

door

Hendrik Willem Christiaan POSTMA

doctorandus in de natuurkunde
geboren te Brielle.

Dit proefschrift is goedgekeurd door de promotor:
Prof.dr. C. Dekker

Samenstelling promotiecommissie:

Rector Magnificus,	voorzitter
Prof.dr. C. Dekker,	Technische Universiteit Delft, promotor
Prof.dr. C.W.J. Beenakker,	Universiteit Leiden
Prof.dr. L. Glazman,	University of Minnesota, Verenigde Staten
Prof.dr. N.F. van Hulst,	Universiteit Twente
Prof.dr.ir. L.P. Kouwenhoven,	Technische Universiteit Delft
Prof.dr. J.M. van Ruitenbeek,	Universiteit Leiden
Prof.dr. C. Schönenberger,	University of Basel, Zwitserland
Dr. H. Bouchiat,	Université Paris-Sud, Frankrijk

Published and distributed by: DUP Science

Dup Science is an imprint of
Delft University Press
P.O. Box 98
2600 MG Delft
The Netherlands
Telephone: +31 15 2785678
Telefax: +31 15 2785706
E-mail: DUP@Library.TUDelft.NL

ISBN 90-407-2258-7

Keywords: Carbon nanotubes, molecular electronics, nanotechnology

The cover shows letters 'C' and J' made from an individual single-wall carbon nanotube molecule by manipulation with an atomic force microscope.

Printed in the Netherlands

Preface

This thesis describes the results of experiments performed during the last four years in the Department of Applied Physics at Delft University of Technology in the Netherlands. When I started this Ph.D. research on nanotube transport properties, many aspects of nanotubes were known, or so it seemed. In hindsight, the collective knowledge of nanotubes has increased tremendously during these four years, and it was an exciting experience to contribute a little to that. This thesis would, however, not have been possible without the constant support of many people.

First of all, I would like to thank my supervisor Cees Dekker. You taught me many things about physics, academia, writing and presentations, but mostly to tackle any problem with enthusiasm. I would like to thank Hans Mooij for generating the right research climate to study mesoscopic physics. I enjoyed being a part of two excellent research groups, of whom I thank Serge Lemay, Leo Kouwenhoven, Herre van der Zant, Kees Harmans, Peter Hadley, Ria van Heeren, Anja Bartels, Pieter Heij, Michael Janus, Hannes Majer, Alexander ter Haar, Leonid Gurevich, Liesbeth Venema, Alberto Morpurgo, Keith Williams, John van Noort, and my 'fellow OLA warriors' Jorg Janssen and Wilfred van der Wiel. I thank my room mates Sander Tans, who kick-started the nanotube transport project, Tjerk Oosterkamp, Caspar van der Wal, Erik Svenson, Arnold Storm, and Frank Wiertz for creating a friendly environment. Sami Sapmaz, Pablo Jarillo-Herrero, Jeong-O Lee, and Günther Philipp, I wish you lot's of fun. I especially thank Zhen Yao and Adrian Bachtold, two very good postdocs that I had the pleasure to work with.

None of these experiments would have succeeded without the technical infrastructure created and maintained by Raymond Schouten, Bram van der Enden, Dick Korbee, Jack Tekelenburg, Mascha van Oossanen, Leo Lander, Willem den Braver, Wim Schot, and the constant support in DIMES by Anja Suurling, Marc Zuiddam, Arnold van Run, and Emile van der Drift.

It was a pleasure to coach undergraduate students in their final year before graduation. Allard Sellmeijer, we started nanotube manipulation and got it working quite fast. It has now become a very important tool; just have a look at the cover of this thesis. Mark de Jonge, your hard-core science attitude paid off with very good results. Tijs Teepen, your no-nonsense approach to research as well as

everyday life was very refreshing.

There were many discussions with theoreticians both from 'upstairs' as well as abroad. I would like to thank Arkadi Odintsov, Yuli Nazarov, Gerrit Bauer, Leon Balents, Leonid Glazman, and Matthew Fisher. In the final year, two people joined the Bauer group whom I would like to thank in particular. Milena Grifoni and Michael Thorwart, I enjoyed working closely with you. Again I apologize for not having any Hamiltonians or bosonization lingo in this thesis.

I thank my friends Ingrid, Bert, Beverly, Herre-Jan and the friends from Thaleia, in particular Makaria, Joeri, Gerard, Tom, Bart and Bart, Cyril, and Arjan for always enough fun and asking nasty questions. Sebastiaan, I miss your support and friendship dearly. I thank my two 'paranimfen' Bert Hubert and Friso Postma for being there when the day comes. I thank my family and especially my parents, brother, and sister for their constant attention and advice. Finally, I thank my partner Annegreet for simply being the wonderful person she is.

Henk Postma
Delft, October 2001.

Contents

Chapter 1

Carbon nanotubes

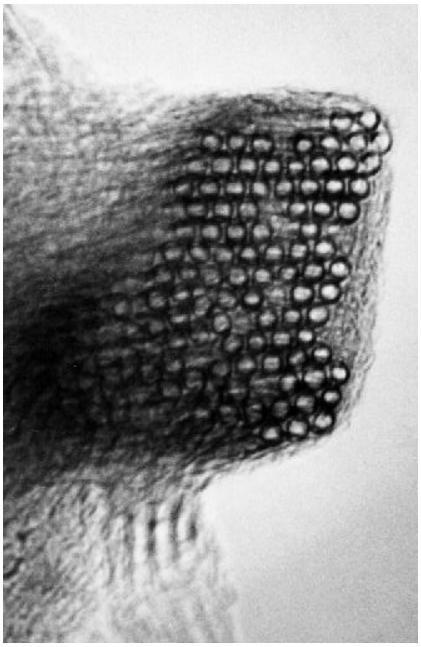

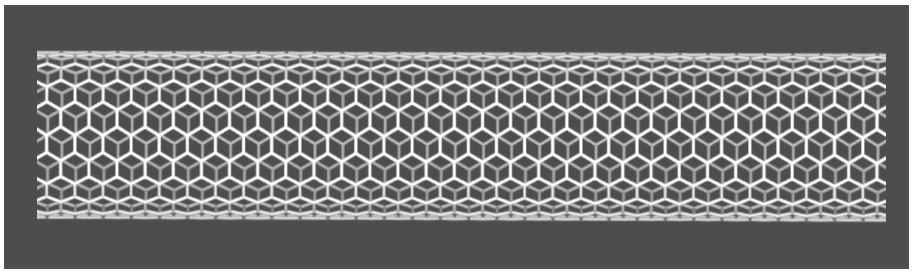

Figure 1.1: A single-wall carbon nanotube molecule. Image : `http://cnst.rice.edu`

Abstract: Carbon nanotubes are molecules entirely made of carbon atoms. Owing to their special shape, they are extremely stiff but also very flexible. The electronic properties are determined by the exact symmetry of the nanotube lattice, resulting in either metallic or semiconducting behavior. Due to their small diameter, electronic motion is directed in the length direction of the nanotube, making them ideal systems to study e.g. one-dimensional transport phenomena.

1 Introduction

Carbon nanotubes were discovered in 1991 by S. Iijima [1]. They are molecules entirely made of carbon atoms. Initially, Iijima discovered a variety of nanotubes consisting of multiple coaxial cylinders, known as multi-wall nanotubes. Later, however, both Bethune *et al.* and S. Iijima and T. Ichihashi discovered that under specific synthesis conditions, single-wall nanotubes may be formed (Fig. 1.1) [2,3]. This variety is studied in this thesis. After their discovery, scientists from a wide variety of disciplines became fascinated in their properties. The reason for this broad interest can be understood from the fact that nanotubes combine several unique properties which were incompatible in the pre-nanotube age.

Firstly, the atomic lattice structure of nanotubes is associated with a high mechanical stiffness as well as a great flexibility. Because nanotubes are highly symmetric molecules linked by many covalent bonds which are in a parallel cylindrical configuration, nanotubes are both very flexible and very strong. For instance, the Young's modulus is above 1 TPa [6], which is among the highest in the world. Regarding the flexibility, nanotubes can be bent strongly without breaking. Together with their high aspect ratio, this makes them ideal candidates

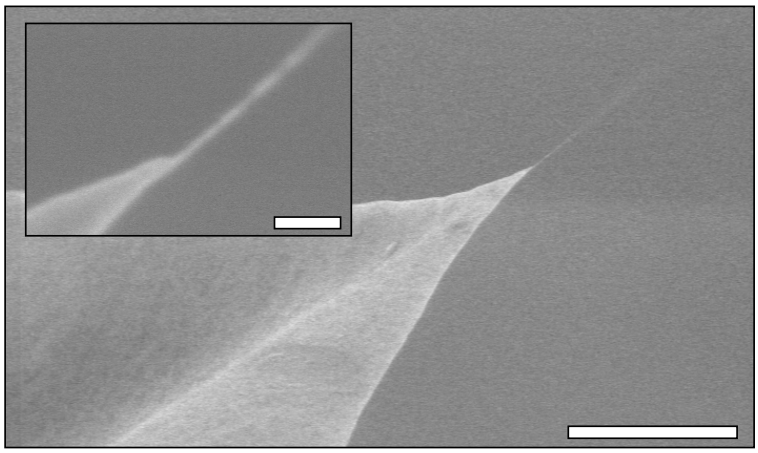

Figure 1.2: Scanning electron microscope image of a single-wall carbon nanotube protruding from the end of an atomic force microscope tip. The nanotubes were directly grown on the AFM tip by the chemical vapor deposition technique [4]. The scale bar represents 1 μm. The inset shows an enlarged scan (scale bar 50 nm). T.F. Teepen *et al.*, unpublished results, TU Delft.

for tips of scanning probe microscopes like the atomic force microscope (AFM), see e.g. Fig. 1.2. If, by bending, the built up strain is increased beyond a critical point, however, the strain localizes in a buckled structure (see Fig. 1.3). In the macroscopic world of plumbing and drinking straws, we are used to the fact that buckling of cylindrical structures leads to induced dislocations or even fracture. On that scale, buckling is thus not reversible. By contrast, buckling of carbon nanotubes is reversible! The influence of buckling on the electrical properties has very interesting surprises (see chapters 5 and 6). This is a nice example of how the unique and diverse properties of nanotubes can be combined to create interesting science.

The electrical properties of nanotubes are even more spectacular than the mechanical properties. Depending on the exact arrangement of the carbon atoms, nanotubes can be either semiconducting or metallic. This has inspired scientists coming from the field of molecular electronics, who study electrical properties of single molecules because of their natural small size. Combined with the chemical toolbox available for synthesis, it enables one to ultimately reduce the size of electronic components. The first electronic transport measurements revealed that at low temperatures, nanotubes act as single-electron transistors [7, 8]. After that, it was found that a semi-conducting tube functions as a single molecule

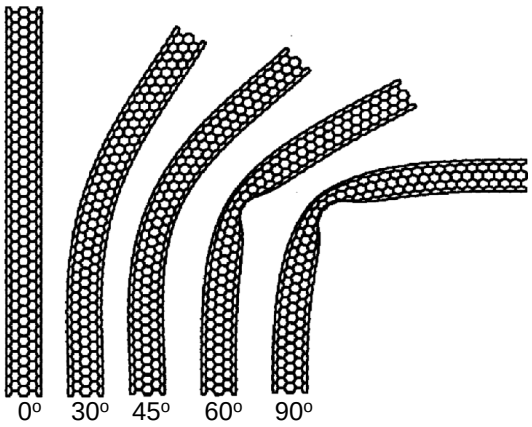

Figure 1.3: Model of a carbon nanotube which is bent at angles as indicated until it buckles. Reproduced from [5].

field-effect transistor at room temperature [9]. Carbon nanotubes are therefore ideal candidates for molecular electronics.

The metallic variety of single-wall nanotubes seems to be of particular interest. In a recent experiment, it was shown that metallic carbon nanotubes are in fact ballistic conductors at room temperature [10]. This is unprecedented for metallic conductors, let alone single molecules. In addition, the dominant influence of long-range electrostatic interaction make metallic nanotubes a model one-dimensional system to study Luttinger-liquid phenomena. Many examples of this can be found throughout this thesis. Other interesting fundamental phenomena have been studied by many authors. For instance, it was found that by connecting a nanotube with nearly perfect contacts to metallic leads, the electronic states can interfere with the electrons in the leads to form a Kondo system [11].

In this brief introduction we have described the electrical and mechanical properties, because they are the prime properties studied in this thesis. There are many other interesting aspects of nanotubes. As a final example, chemical functionalization of ends of nanotubes mounted on AFM tips can be used to study local chemical properties of anything that can be imaged with an AFM [12].

2 Electrical properties

The band structure of carbon nanotubes can be derived from the band structure of single sheets of graphite, known as graphene. The idea is as follows [13, 14].

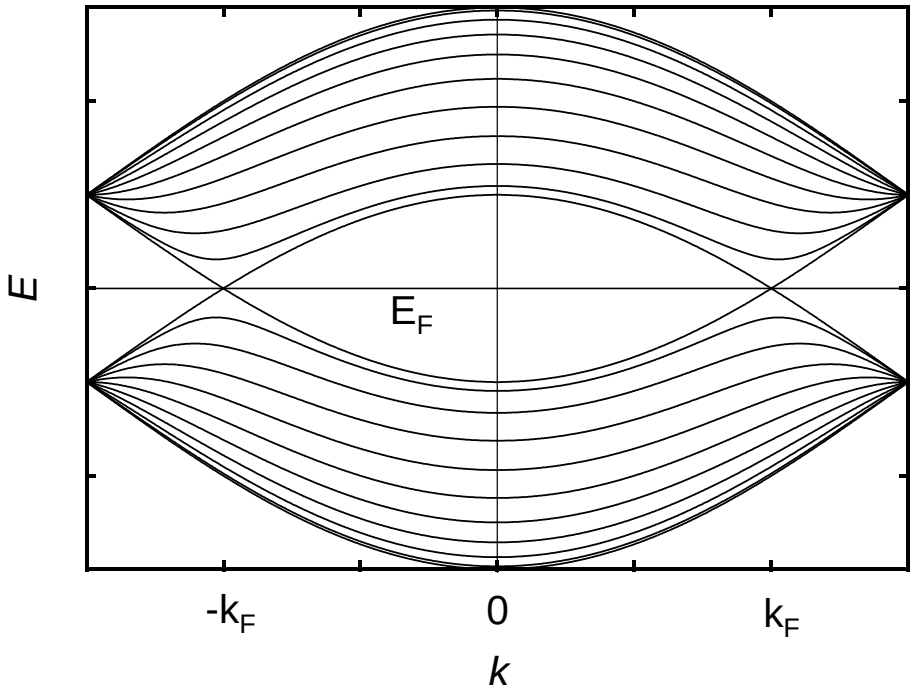

Figure 1.4: Typical band structure for a metallic carbon nanotube of 1.4 nm diameter. Shown are the one-dimensional subbands which result from the periodic boundary conditions in the circumferential direction. Due to the special symmetry of this nanotube, two bands cross the fermi level E_F rendering this nanotube metallic.

A carbon nanotube is thought of as a rolled up graphene sheet. The band structure of graphene has only six Fermi points where the bonding and antibonding bands meet [15]. If the electron motion in the circumferential direction is not subject to any dephasing mechanisms, the electronic wavefunction has to satisfy periodic boundary conditions in the circumferential direction, leading to a quantization of the circumferential wavenumber. Depending on the exact manner in which the graphene lattice can be mapped onto the nanotube structure, the lines with allowed values for the electron wavenumber will or will not cross the Fermi points. In the first case, a metallic tube is realized, whereas in the second case a semiconducting tube is found. An example of the band structure of a metallic nanotube is shown in Fig. 1.4.

At low energy ($|E - E_F| \ll 1$ eV), the conduction bands of metallic tubes are linear around the crossing point with a dispersion relation $E = \pm\hbar v_F k$ as indicated in Fig. 1.5, where $v_F = 8.1 \times 10^5$ m/s denotes the Fermi velocity and k is the axial electron wavenumber. In a recent experiment performed in our

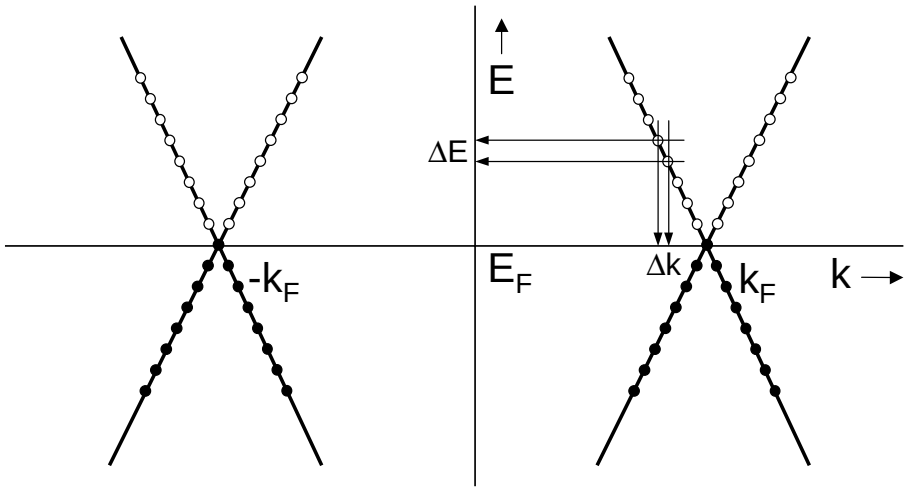

Figure 1.5: Low-energy band structure of a metallic carbon nanotube, revealing linear bands. In a nanotube of finite length, k is quantized which leads to a set of quantized energy levels as indicated. At low temperatures, all the levels are filled (•) up to the fermi level, which for this example is chosen at the crossing point. The levels above E_F are empty (∘).

group, the existence of these linear bands as well as the value of v_F was experimentally verified [16]. In the transport experiments described in this thesis, this one-dimensional nature affects the results in two distinct manners, namely 1. a quantum energy level separation that does not depend on the number of electrons in the nanotube (see below) and 2. Luttinger liquid phenomena (see §4).

In a carbon nanotube with a finite length L, the wave number k in the length direction is quantized (assuming no dephasing), i.e. $k_n = \pi n/L$. With the dispersion relation $E = \pm\hbar v_F k$, this leads to a quantized set of energy levels $E_n = \pm h v_F n/2L$ separated by an energy difference $\Delta E = h v_F/2L$. In this picture, the energy values E_n on all branches of the dispersion relation are degenerate. This simple picture does not hold in general, however. In fact, the two forward and backward oriented bands can mix by reflection at the nanotube ends [17]. This mixing causes a splitting between the energy levels in two sets of levels, which are shifted with respect to each other by an amount δE. The value of δE depends on the exact boundary conditions at the nanotube ends. The two sets are individually still separated by ΔE. This energy level separation is observed in a coulomb blockade measurement.

3 Coulomb blockade

The experiments described in this thesis are performed on carbon nanotubes connected to metallic electrodes. It is difficult to make a perfect adiabatic contact between the electrodes and a nanotube. Therefore the nanotube resistance in experiments is often orders of magnitude larger than the quantum resistance of $h/4e^2 \approx 6.5$ kΩ expected for nanotubes. The theoretical framework for a small conducting island connected by weak links to electrodes is well established and is generally known as the theory of Coulomb blockade [18]. The central idea is that if the thermal energy is smaller than the energy required to add a single electron to the island E_{add}, current is blocked, except for special situations. The smaller the conductor is, the larger this addition energy will be. With the rapid growth of methods to design sub-micrometer structures during the last two decades, samples have been fabricated with a charging energy of the order of typically millielectron volts, opening up this regime to experimentalists working at a few Kelvin and lower. By contrast, in chapter 6, we describe experiments where we have observed Coulomb blockade at room temperature.

A typical device layout is schematically drawn in Fig. 1.6. For simplicity, we assume that the contacts to the nanotube behave as tunnel barriers. In order to run a current through the system, electrons have to be added to and removed from the nanotube. In doing so, all capacitors connecting the nanotube to the surroundings (indicated by C_L, C_R, C_{gate}, and C_{stray}) have to be charged and uncharged. For a single electron, the addition energy associated with this process reads $E_{add} = e^2/C_\Sigma$, where $C_\Sigma \equiv C_L + C_R + C_{gate} + C_{stray}$. For small conductors, i.e. with a small C_Σ, this single-electron addition energy is very large compared to the thermal energy k_BT, where k_B is Boltzmann's constant and T is the absolute temperature. It turns out that current is blocked in this regime, the so-called 'Coulomb blockade', and the number of electrons on the nanotube is fixed at, say, n. The blockade can be lifted by adjusting the electrostatic potential of the nanotube by means of the capacitively coupled gate. Then, a single electron can tunnel onto and off the tube and current can flow. Increasing the gate voltage further, however, blocks the current again and the number of electrons is fixed, but now at $n + 1$. In between these two ground states, a resonance peak in the conductance is observed. Because the conductance can be turned 'on' and 'off' by means of a third terminal, this device is called a single-electron transistor.

When the thermal energy k_BT is smaller than the quantum energy level sep-

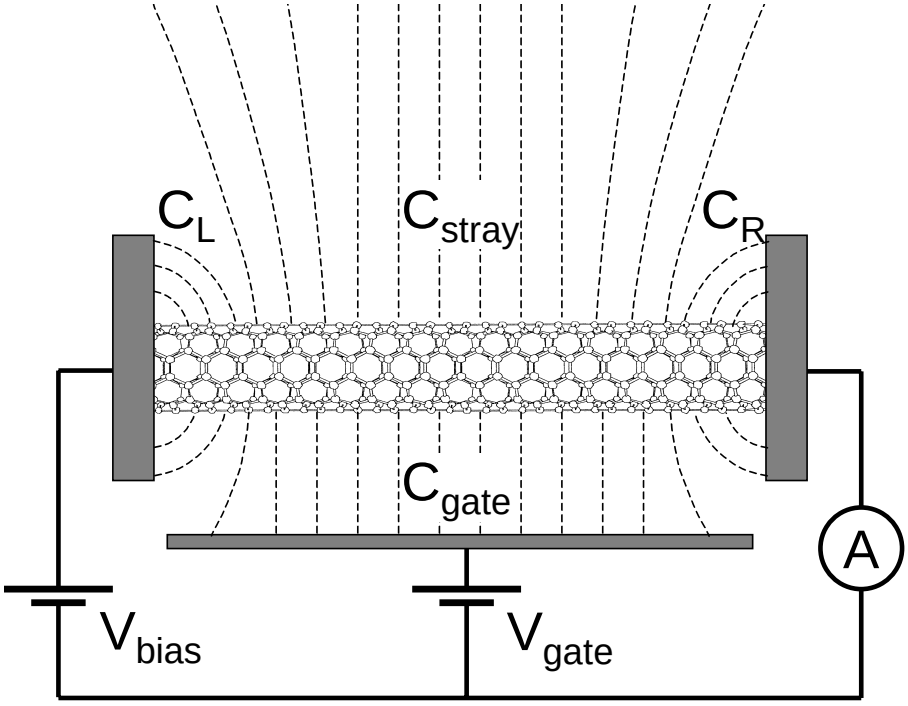

Figure 1.6: Schematic drawing of a typical measurement layout of a nanotube connected with bias- and gate-voltage sources and a current meter as indicated. The capacitive coupling between the nanotube and surrounding is decomposed in four separate capacitors. The dashed lines indicate electric field lines.

aration ΔE, another interesting situation arises. Adding individual electrons to the nanotube now also requires supplying this energy (Fig. 1.5). The addition energy for individual electrons thus becomes $E_{add} = e^2/C_\Sigma + \Delta E$. With a Coulomb blockade experiment, we can thus probe the energy of electronic quantum states confined to the nanotube. This is experimentally observed in chapters 2 and 6.

4 Luttinger-liquid model

Carbon nanotubes have a very small diameter (~ 1 nm). This has a very profound effect on the electrostatic screening properties which is most easily demonstrated by a comparison to the situation in a three-dimensional metal. In the latter case, if one electron is moved slightly from its equilibrium position, all the surrounding electrons can rearrange themselves to screen the change in the electric field. In this manner, the long-range electron-electron interaction is screened effectively by the excitations of plasmons in the surrounding electron system. In the case

of a carbon nanotube, there are no electrons surrounding the electron under consideration on a length scale larger than the diameter. So, while the short-range electron-electron interaction is screened due to the finite diameter, the long-range interaction is not.

This intuitive picture does not capture the full complexity of the 1D case. We again compare to the 3D case. There, the Pauli principle, combined with energy and momentum conservation cooperate to generate a very large lifetime for the electron states. To qualitatively understand this, we consider electron-electron scattering processes between pairs of electrons. Consider an electron above the fermi level with energy energy $E_1 > E_F$ and momentum $\vec{k}_1$. By scattering off an electron below the fermi level with energy $E_2 < E_F$ and momentum $\vec{k}_2$, they can scatter into states with energy $E_{3,4}$ and momentum $\vec{k}_{3,4}$. Both energies E_3 and E_4 must be larger than the fermi energy, since all states below the fermi level are occupied. Then energy and momentum conservation for the total process

$$E_1 + E_2 = E_3 + E_4 \quad \text{and} \quad \vec{k}_1 + \vec{k}_2 = \vec{k}_3 + \vec{k}_4$$

reduce the phase space available for these scattering processes. When E_1 approaches the fermi level, all these scattering processes freeze out, and the electron lifetime becomes very large. In 1D, the situation is dramatically different, since these two separate conservation laws are essentially the same. Therefore, the electron lifetime vanishes.

It turns out that electron states are no longer well defined. Instead, the 1D system is described in terms of plasmons and this system is called the Luttinger liquid [19–21]. As a consequence of the long-range electrostatic interaction, however, the plasma velocity $v_\rho \equiv v_F/g$ is larger than the fermi velocity v_F. The Luttinger parameter g characterizes the strength of the electron-electron interactions, which can be estimated from

$$g = \frac{1}{\sqrt{1 + 2e\hat{V}_0/hv_F}} \quad .$$

Here, $\hat{V}_0$ represents the long-range component of the coulomb interaction. For no interaction, $\hat{V}_0 = 0$, we find $g = 1$, whereas for very strong interaction, $2e\hat{V}_0 \gg hv_F$, we find $g = 0$. Throughout this thesis, values for g are found in the range of 0.2 – 0.3. One can calculate that it suffices to simply replace v_F by v_ρ to obtain the dispersion relation of a Luttinger liquid,

$$E = \pm\hbar v_\rho k \quad .$$

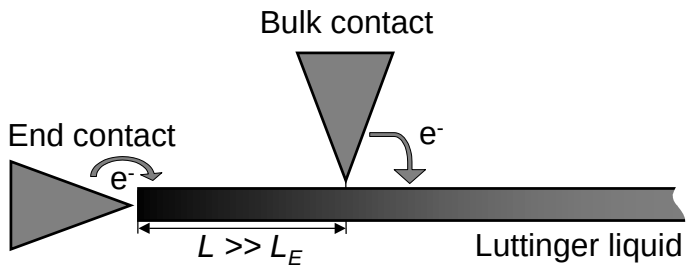

Figure 1.7: Schematic representation of metallic tips in tunneling contact with a Luttinger liquid. We distinguish between two tunneling positions, a bulk and an end contact.

Up to this point, we have neglected the spin excitations in a Luttinger liquid, which exist next to the plasmons we mentioned above. These spin excitations, however, are not affected by the electrostatic interaction and their velocity v_σ remains the same as in the non-interacting case, i.e. $v_\sigma = v_F$. This implies that after an electron tunnels into a Luttinger liquid, the spin and charge information propagate with different velocity. The effect is known as spin-charge separation.

Luttinger liquid behavior is observed in the following experimental situation (Fig. 1.7). In a tunneling transport experiment, the differential conductance dI/dV reflects the probability for electrons to tunnel into the LL by exciting plasmons. At zero energy, this process is suppressed completely. With increasing energy, the probability increases as a power law

$$\frac{dI}{dV} \propto E^\alpha \qquad ,$$

where E denotes the energy available for transport. The exponent α depends on the strength of the electron-electron interactions via g, but also depends on the position of tunneling, as indicated in Fig. 1.7. When electrons are added to the end of the nanotube, plasmons are excited in one direction only and the tunnel conductance is suppressed strongly with an exponent $\alpha_{end} = (1/g - 1)/4$. Tunneling into the bulk of the nanotube is more weakly suppressed, with $\alpha_{bulk} = (1/g + g - 2)/8$, since plasmons are now excited in both directions away from the contact.

What distinguishes a bulk from an end contact? Consider a contact located a distance L away from the end of the nanotube, see Fig. 1.7. In order for this contact to qualify as a bulk contact, it must be possible to excite plasmons in the segment between the contact and the end. As we noted above in §2, the

momentum k in such a finite system becomes quantized, which in its turn leads to energy quantization with a separation $\Delta E = hv_F/2L$ [22]. If the energy available for transport E is lower than this, excitation of plasmons is not possible and therefore this is an end contact. If, however, E is larger, this is a bulk contact. Solving for L, we obtain the length that distinguishes a bulk from an end contact $L_E = hv_F/2E$.

Acknowledgments

The image on page 1 is taken from `http://cnst.rice.edu`

References

[1] S. Iijima, *Nature* **354**, 56 (1991).

[2] S. Iijima and T. Ichihashi, *Nature* **363**, 603 (1993).

[3] D.S. Bethune *et al.*, *Nature* **363**, 605 (1993).

[4] J. Kong, H.T. Soh, A.M. Cassell, C.F. Quate, and H. Dai, *Nature* **395**, 878 (1998).

[5] A. Rochefort, D.R. Salahub, and Ph. Avouris, *Chem. Phys. Lett.* **297**, 45 (1998).

[6] M.M.J. Treacy, T.W. Ebbesen, and J.M. Gibson, *Nature* **381**, 678 (1996).

[7] M. Bockrath *et al.*, *Science* **275**, 1922 (1997).

[8] S.J. Tans *et al.*, *Nature* **386**, 474 (1997).

[9] S.J. Tans, A.R.M. Verschueren, and C. Dekker, *Nature* **393**, 49 (1998).

[10] A. Bachtold *et al.*, *Phys. Rev. Lett.* **84**, 6082 (2000).

[11] J. Nygard, D.H. Cobden, and P.H. Lindelof, *Nature* **408**, 342 (2000).

[12] S.S. Wong, E. Joselevich, A.T. Woolley, C.L. Cheung, and C.M. Lieber, *Nature* **394**, 52 (1998).

[13] H. Hamada, S. Sawada, and A. Oshiyama, *Phys. Rev. Lett.* **68**, 1579 (1992).

[14] R. Saito, M. Fujita, G. Dresselhaus, and M.S. Dresselhaus, *Appl. Phys. Lett.* **60**, 2204 (1992).

[15] P.R. Wallace, *Phys. Rev.* **71**, 622 (1947).

[16] S. G. Lemay *et al.*, *Nature* **412**, 617 (2001).

[17] T. Yaguchi and T. Ando, *J. Phys. Soc. Jpn.* **70**, 1327 (2001).

[18] H. Grabert and M. Devoret (eds) in *Single Charge Tunneling* (Plenum, New York, 1992).

[19] S. Tomonaga, *Prog. Theor. Phys.* **5**, 544 (1950).

[20] J.M. Luttinger, *J. Math. Phys.* **4**, 1154 (1963).

[21] F.D.M. Haldane, *J. Phys. C* **14**, 2585 (1981).

[22] In principle, the energy quantization becomes a factor $1/g$ larger because the dispersion relation has a renormalized velocity v_ρ. Because this is just a crossover argument, we neglect this here.

Chapter 2

Electron addition and excitation spectroscopy of an individual single-wall carbon nanotube molecule

H.W.Ch. Postma, Z. Yao, and C. Dekker

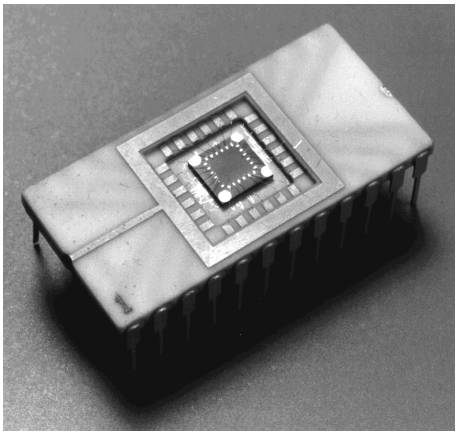

Abstract: We present mK-temperature non-linear current-voltage characteristics of an individual single-wall carbon nanotube as a function of magnetic field. The measurements show Coulomb blockade and resonant tunneling through single molecular levels. Correlations between the addition spectrum and the excitation spectrum are observed. The magnetic field dependence of the addition and excitation spectra is discussed.

1 Introduction

Carbon nanotubes are conducting molecules with either semi-conducting or metallic electronic properties [1]. The combination of their long length of several micrometers and small nanometer diameter make them ideal candidates for studying the effects of one-dimensional confinement of the electrons on their transport properties.

Previous studies of carbon nanotubes have shown that their low-temperature transport properties can be described by Coulomb blockade theory [2–4], where the thermal energy k_BT is smaller than the charging energy of the nanotube $E_C \equiv e^2/2C_{tube}$. In the quantum regime at lowest temperature, the single-particle level spacing ΔE can be resolved, i.e. $k_BT < \Delta E < E_C$, in contrast with the classical regime at higher temperature, where $\Delta E < k_BT < E_C$ [5]. It has been shown that the value of ΔE is equal to the expected 'particle-in-a-box' energy level separation of electrons confined to the nanotube [3]. The magnetic field dependence of the molecular energy levels of carbon nanotubes is dominated by the spin degree of freedom. This Zeeman effect has been observed both in ropes [4](bundles of nanotubes) and in individual nanotubes [3, 6]. The corresponding filling of single-particle levels however appears not to be straightforward. Both singlet-doublet [4] as well as spin-polarized filling [6] have been observed.

Coulomb blockade phenomena in small confined systems, where the two energy scales E_C and ΔE are both important, have been well studied [7]. The energy one needs to apply to add an electron to the nanotube is $e^2/C + \Delta E = 2E_C + \Delta E$ [5]. When the thermal energy is lower than this, current through the system is blocked. The blockade can be lifted, however, by changing the electrostatic potential of the nanotube, e.g. by applying a voltage on a nearby gate electrode that is coupled capacitively to the nanotube. At that point, current is allowed to

flow and a conductance peak is observed. As the gate voltage is changed further, a series of conductance peaks will become visible. In between these, the number of electrons is fixed. Whenever a peak is crossed, the number of electrons on the nanotube changes by one. The single-particle level spacing may be different for different numbers of electrons on the nanotube. This will lead to a variation in the distance between the conductance peaks $\Delta V_{gate} = (2E_C + \Delta E_n)/e\alpha$, where $\alpha \equiv C_{gate}/C_{tube}$ is the capacitive coupling of the nanotube to the gate and n is the number of electrons on the nanotube. We thus obtain the variation of addition energy with number of electrons and this is called the addition spectrum. It is related to the energy difference between consecutive ground states of the nanotube.

The blockade can also be lifted by raising the bias voltage. The two bias electrodes are coupled to the nanotube by tunneling contacts, but also capacitively. In a differential conductance measurement as a function of bias and gate voltage, the combination of both voltages leads to the well-known Coulomb blockade diamonds in the (V_{gate}, V_{bias}) plane, with corner points $(v_n \pm \Delta V_{gate}/2, 0)$ and $(v_n \pm \delta V_{gate}, \pm\Delta V_{bias})$ [7]. Here v_n is a constant and $\delta V_{gate} < \Delta V_{gate}/2$ is an asymmetry parameter which depends on the exact values of all capacitances to the nanotube [1]. Within this diamond, current is blocked and the number of electrons is fixed. The 'width' of this diamond is the distance ΔV_{gate} between the conductance peaks mentioned above. From the ratio of the 'height' ΔV_{bias} to the 'width' ΔV_{gate}, we can find $\alpha = \Delta V_{bias}/\Delta V_{gate}$.

The energy levels of the nanotube are also accessible in another way. At the point where the Coulomb blockade has been lifted by increasing the bias voltage, transport through the nanotube can take place because a molecular energy level is inside the window created by the applied bias voltage. The occupation of the nanotube then oscillates between say n and $n + 1$. When the bias voltage is increased further, a higher lying energy level can enter the bias window. Now, electron transport can also take place via this level. The increased probability in transferring electrons leads to a stepwise increase in the current and a peak in the differential conductance. Note, however, that the occupation of the nanotube still oscillates between n and $n+1$. Because the next energy level is higher in energy then the ground state which was already contributing to the transport, this level is called an excited state. If the capacitive coupling of this excited state to the

[1] Here $\Delta V_{bias}, \Delta V_{gate} \geq 0$ and $-\Delta V_{gate}/2 \leq \delta V_{gate} \leq \Delta V_{gate}/2$

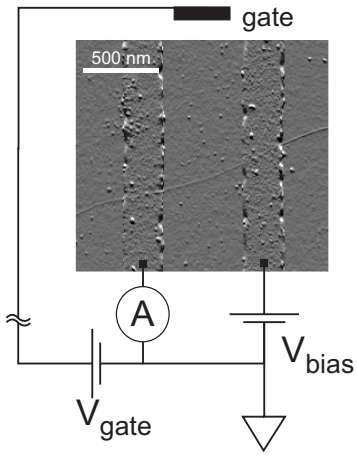

Figure 2.1: Tapping-mode AFM amplitude image of the nanotube, lying over two electrodes. The length of the nanotube segment in between electrodes is 540 nm while the total length is about 3 μm. The gate electrode is not visible in the AFM image and is indicated schematically. The bias voltage is applied asymmetrically.

bias and gate electrodes is equal to that of the ground state, these excited states are visible as lines running parallel to the sides of the diamond. The distance in gate voltage between this line and the side of the diamond is $\Delta E/e\alpha$. A collection of excited states in the nanotube will give rise to a collection of extra lines. Since we can now determine the energies of the excited states of the nanotube, this collection is called the excitation spectrum.

Within the constant interaction model [8], the excited states of the nanotube are simply the energy levels of the next ground states, as visible in the addition spectrum. The addition and excitation spectra are thus simply related. Although the extension of this idea to correlated systems where electron-electron interactions are important is not trivial, support for its validity in quantum dots has been reported [9].

In this chapter, we present measurements of the addition and excitation spectra of a carbon nanotube and discuss the correlations between these. The magnetic field dependence of the states is reported as well.

2 Sample description

Single-wall carbon nanotubes were produced by the group of R.E. Smalley at Rice university, USA [10]. A small amount of this raw material is ultrasonically

dispersed and spin coated on top of a SiO_2/Si-substrate containing a large array of predefined Pt electrodes. These electrodes are fabricated using a double layer (PMMA/MAA) resist, electron beam lithography, Pt evaporation and lift-off. The resulting electrodes are 20 nm high, 250 nm wide and 8 μm long and are separated from each other by 500 nm. The gate electrode is placed perpendicular to the other electrodes and separated from the ends by 2.5 μm. After deposition of the nanotubes, adjacent pairs of electrodes are checked for conduction due to the nanotubes, which corresponds to a typical resistance of 1 to 10 MΩ. The metallic nature of the nanotube is established by checking that the conductance cannot be modulated by a gate voltage [11]. Single nanotubes are selected by their apparent height of 1.4 nm or less in Atomic Force Microscopy (see [12] and chapter 4).

A tapping-mode AFM picture of the sample that is being studied in this chapter is shown in Fig. 2.1, along with a schematic view of the electrical connections. The segment of this nanotube between electrodes is 540 nm, while its full length is about 3 μm. The room temperature resistance of this sample is 4 MΩ and increased upon decreasing the temperature. It was cooled down in a dilution refrigerator with a base temperature of 5 mK.

3 Experimental results and discussion

We have measured the current through the nanotube as a function of V_{bias} and V_{gate}. Typical I – V_{bias} curves are shown in Fig. 2.2. Around zero bias voltage, the current is blocked by Coulomb blockade. At higher bias, the blockade can be overcome and a step in the current is observed. Increasing the bias voltage further, beyond a point that is set by the level spacing and the values of all capacitances, current through the nanotube can also flow through a next level and another step in the current is observed.

Additional features can be seen in the positive bias part of the curve obtained at $V_{gate} = -225$ mV. Here peak structures are observed in addition to the steps. This peak-like structure leads to negative differential conductance (NDC). Several mechanisms may lead to this NDC. For example, one possibility is residual carbon particles from the raw material, which may be lying between the nanotube and the contacts. Whenever one of the energy levels of this particle crosses the bias window, a peak in current is observed. In a conductance spectrum, the positions

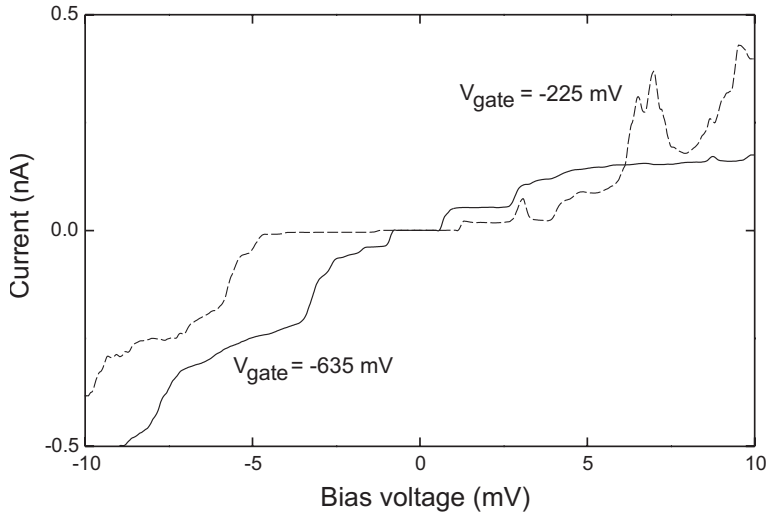

Figure 2.2: Bias voltage dependence of the current through the nanotube at the two indicated values of the gate voltage. Around $V_{bias} = 0$, current is blocked by Coulomb blockade. The plateaus in the current are due to resonant tunneling through molecular energy levels. Peaks are oberved as well (see discussion in text).

of NDC will not shift in a similar manner as the excited states, because the capacitive coupling of this particle with the leads and gate electrode can be expected to be very different. We will not discuss these effects any further here.

Figure 2.3 shows the current through the nanotube as a function of gate voltage. A series of peaks is visible. In between these, the current is blocked by Coulomb blockade, and the number of electrons on the nanotube is fixed. The distance in gate voltage between peaks is $(2E_C + \Delta E_n)/e\alpha$.

One of the conductance peaks is examined in more detail as a function of temperature in Fig. 2.4. The solid lines are fits with $G = G_0(T)/\cosh^2(V_{gate}/2w(T))$ [5], where $w \equiv k_B T/e\alpha$ and $\alpha \equiv C_{gate}/C_{tube}$. The left and right insets show the obtained inverse maximum conductance, $1/G_0$, and width, w, versus temperature, respectively. Both are fit with a linear function. From the linear fit of the width versus temperature we obtain $1/\alpha = 35 \pm 5$. The fact that the maximum conductance is proportional to $1/T$ is evidence for resonant tunneling through single molecular levels [5]. A continuum of levels would lead to a constant maximum [5].

We have measured current through the nanotube as a function of V_{gate} and V_{bias} and differentiated this numerically. The differential conductance spectrum

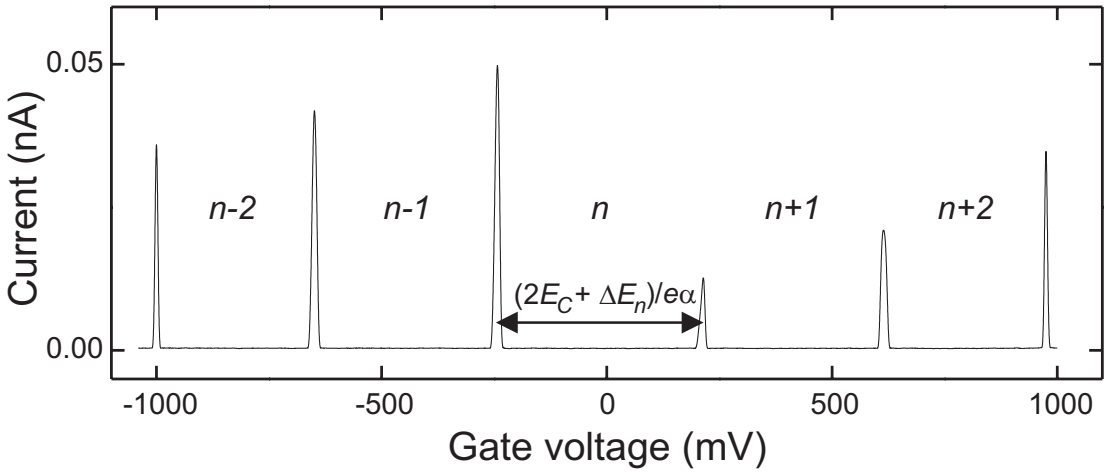

Figure 2.3: Current through the nanotube as a function of gate voltage at $V_{bias} = 400$ μV. A series of conductance peaks is clearly visible.

we thus obtain is shown in Fig. 2.5a. The large light grey areas are the Coulomb diamonds mentioned earlier, the regions where current is blocked. Lines with the same direction appear to be parallel. From the ratio of ΔV_{bias} to ΔV_{gate} we find $1/\alpha = 35 \pm 2$, in good agreement with the value found earlier. Several boundaries of the diamonds appear to have small kinks at $V_{bias} \approx -5$ mV (see in particular the $n+1$ diamond). Here the slope changes by 20 to 30 %. These kinks have been observed before and can be taken as a signature of ground-state to ground-state transitions due to electron-electron correlations [6].

The lines running parallel to the boundaries of the diamonds can be associated with excited states. They are separated from the boundaries by $\Delta E/e\alpha$ in the gate voltage direction. Viewed from the ground state of occupation $n-1$ we identify an excited state running parallel to the border at positive bias voltage and at the high gate voltage side. This state is associated with transport through the first excited state and must thus be correlated with the width of the next coulomb diamond (occupation n) which in the simplest model is $(2E_C+\Delta E_n)/e\alpha$. At the lower gate voltage side another excited state can be seen. This is associated with depletion of the nanotube through the lower-lying level and thus must be correlated with the diamond with occupation $n-2$.

We have examined several excited states in a similar fashion, focussing on those positions in the diagram where these can be identified unambiguously. In Fig. 2.6 we have plotted the distance in gate voltage between ground state and excited state versus the corresponding diamond width. The addition and exci-

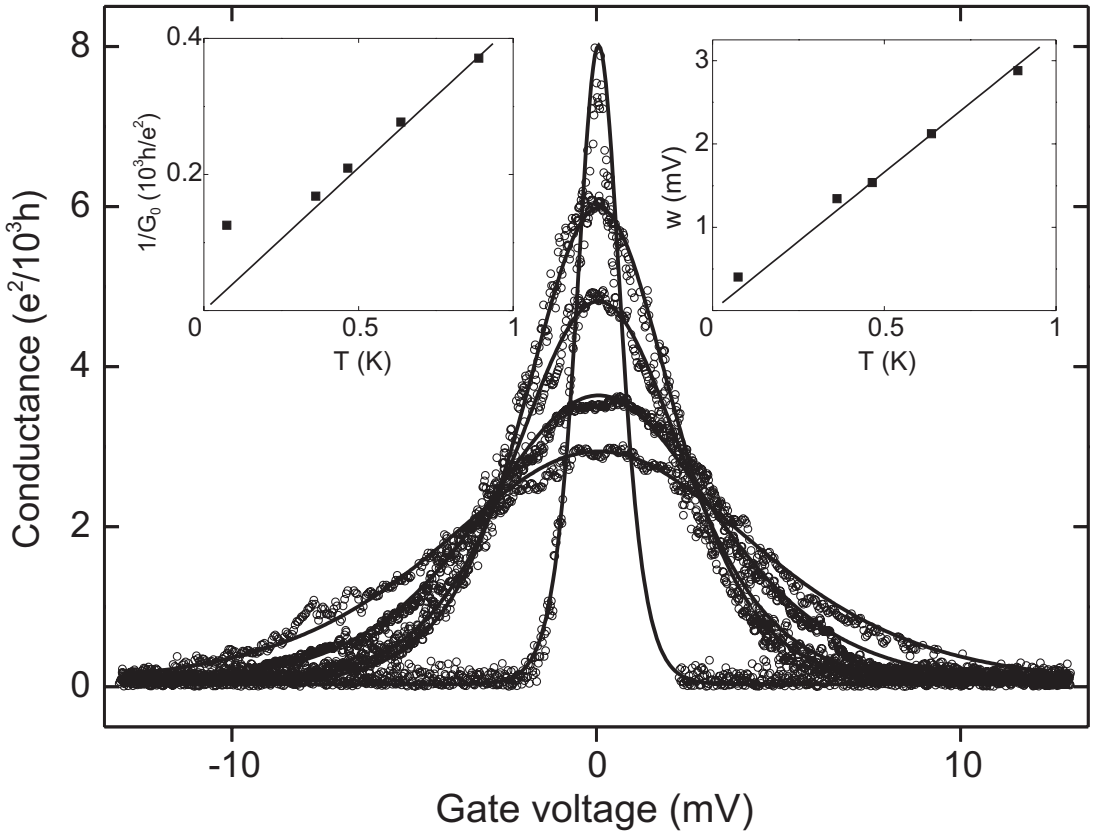

Figure 2.4: Linear conductance of the nanotube as a function of gate voltage and temperature at $V_{bias} = 10\,\mu$V. Shown is the transition from $n-2$ to $n-1$ at temperatures of 74 (sharpest), 362, 465, 637 and 889 mK (widest). The solid lines are fits with $G = G_0(T)/\cosh^2(V_{gate}/2w(T))$, where $w \equiv k_B T/e\alpha$. The insets show the obtained inverse maximum conductance $1/G_0$ and width w as a function of temperature. The deviation at the lowest temperature is probably due to the finite bias voltage (10 μV corresponds to 120 mK) and a higher effective electron temperature.

tation spectra are clearly linearly related. Note that this is a remarkable effect in the case of carbon nanotubes where electron-electron interactions are important [6, 13, 14]. The slope of the linear fit, however, is 2.1, i.e. not equal to the value of 1 that is expected from the previous formulæ. It should be noted that this value is independent on any calibration errors in both V_{gate} and V_{bias} since we are comparing distances in V_{gate} only. This deviation is currently not understood, but may be a renormalization due to electron-electron interactions.

Independent of this, we can determine the charging energy from the intersection, $2E_C/e\alpha = 265$ mV, yielding $E_C = 3.8$ meV. The geometrical self-

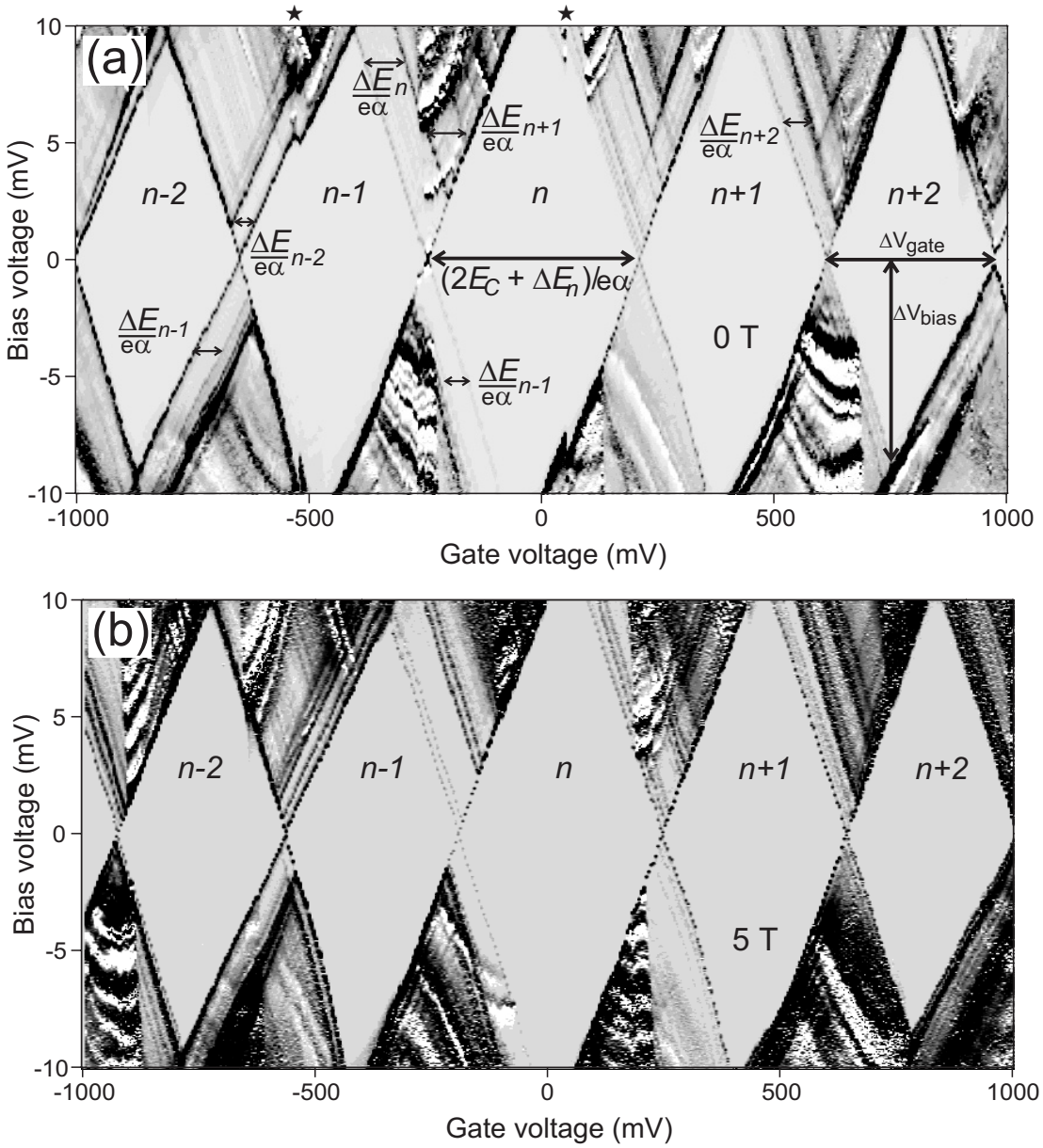

Figure 2.5: Differential conductance (dI/dV_{bias}) spectrum of the nanotube as a function of bias and gate voltage at 0 T (a) and 5 T (b). Light grey tones correspond to $dI/dV_{bias} = 0$. Darker shading corresponds to higher conductance. White regions are positions of NDC, $dI/dV_{bias} < 0$. **a**) $B = 0$ T. The distances in gate voltage from the ground to the first excited state are labeled with $\Delta E_n/e\alpha$. The stars ($\star$) above the graph indicate positions where a sudden shift in the diagram occurs in the gate voltage direction. This is probably due to a switching offset charge that shifts the potential of the nanotube. We have corrected for this effect in determining the width of the diamond. **b**) $B = 5$ T. At the sides used to construct Fig. 2.6, the levels split due to coupling of the magnetic field with spin. Exceptions to this are the sides labelled ΔE_{n-1} in (a).

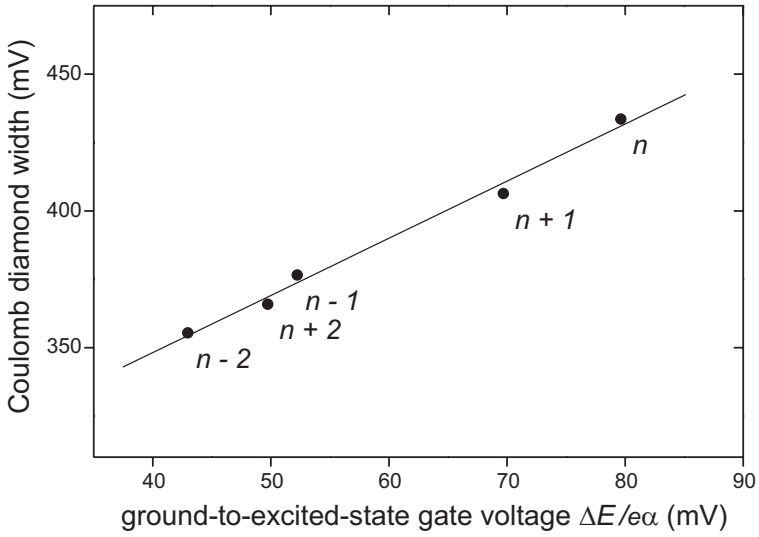

Figure 2.6: Coulomb diamond width, $\Delta V_{gate} = (2E_C + \Delta E_n)/e\alpha$, versus corresponding distance in gate voltage between ground state and excited state, $\Delta E_n/e\alpha$, for various numbers of electrons on the nanotube. The addition and excitation spectra are clearly linearly related. The slope of the linear fit is 2.1. The abscissa yields the value of $E_C = 3.8 \pm 0.2$ meV.

capacitance of the nanotube is $C = 2\pi\epsilon_0\epsilon_r L/\ln(2L/d)$ [15], where $d = 1.4$ nm and L are the diameter and length of the nanotube respectively and ϵ_r is the relative dielectric constant of the surroundings. We thus obtain $L = 3.2$ μm when taking $\epsilon_r = 1$, which is equal to the total nanotube length. This is comparable with earlier experiments in a similar geometry [3, 15].

From Fig. 2.6 we find that the average value of the separation in gate voltage between ground state and excited state in the excitation spectrum (horizontal axis) is 59 mV, which yields $\langle\Delta E\rangle_{exc} = 1.7$ meV. When measured in the addition spectrum, however, we find $\langle\Delta E\rangle_{add} = 3.5$ meV, which is different by a factor 2.1 as expected from the slope of the linear fit. The particle-in-a-box level spacing is given by $\Delta E = hv_F/2L$, where h is Planck's constant and $v_F = 8.1 \times 10^5$ m/s is the Fermi velocity [3]. We thus find a nanotube length of 1.0 μm or 0.50 μm from the excitation or addition spectrum respectively. The calculated length from the charging energy E_C and level spacing ΔE thus do not yield the same value. In order to force them to be equal, we need to set ϵ_r to 2.8 or 5.2 respectively. The relative dielectric constant of SiO_2 is 4.4, which is indeed in this range.

Up to this point, we have neglected spin degeneracy. In a finite carbon nanotube there are two sets of energy levels available, both of which can be filled

with two electrons due to spin degeneracy. If these energy levels are degenerate, we expect the addition spectrum to be a series of $2E_C$, $2E_C$, $2E_C$, $2E_C + \Delta E$, etc. If this degeneracy is not present, we expect the addition spectrum to be $2E_C$, $2E_C + \Delta E$, etc. Neither the first, nor the second is observed in the addition spectra presented here. If two ground-state energy levels for the nanotube with, say, $n-1$ and n are degenerate, this leads to an addition energy of $2E_C$ for n electrons on the tube. In a series of 8 consecutive conductance peaks, the addition energy was always found to be larger than $2E_C$ by at least 2.3 meV. This implies that the spin degeneracy is not present [16]. We can now investigate this issue by applying a magnetic field.

Figure 2.5b shows the conductance spectrum in a perpendicular magnetic field of 5 T. Some of the lines which were identified as excited states as well as some of the ground states appear to have split. This splitting is due to the Zeeman coupling of magnetic field with the spin of the electrons and is equal to $\Delta V_{gate}(B) = g_L \mu_B B / e\alpha$, where μ_B is the Bohr magneton. g_L is the Landé g_L-factor and has been reported to be 2 ± 0.5 [6]. In a similar experiment on ropes [4], a pattern of alternatingly splitting lines and non splitting lines was observed. This is not present in these data.

The evolution of this splitting with magnetic field is examined further in Fig. 2.7a. Shown is dI/dV_{gate} as a function of V_{gate} and B at a fixed bias voltage of 2.5 mV. This graph can be considered as a cross-section at constant V_{bias} of the conductance spectra in Fig. 2.5 where the white colour corresponds to the low gate voltage boundary of the transition between $n-1$ and n. This side shows a linear splitting with magnetic field. From this splitting, we obtain $g_L = 1.9 \pm 0.2$. Measurements on other transitions yield values of g_L of 1.5 to 2.5.

The distance between the lower (white) and the upper (black) boundary of the current stripe in Fig. 2.7a does not change with magnetic field and is equal to $V_{bias}/\alpha = 88$ mV. This current stripe shifts with magnetic field. This shifting is related to the shifting of the zero-bias voltage conductance peak. In Fig. 2.7b we show the position of the zero-bias voltage conductance peak as a function of magnetic field for several consecutive peaks. The shifting of the current stripe of Fig. a is clearly due to the shifting of the conductance peak between $n-1$ and n. In the simplest model, this shifting is equal to $g_L \mu_B B / 2e\alpha$. From this we find values for g_L ranging from 0.2 to 2.8. This is in direct contrast with the values found earlier and cannot be explained within a simple model. Furthermore, the first excited state in Fig. 2.7a is in the simplest model the next ground state,

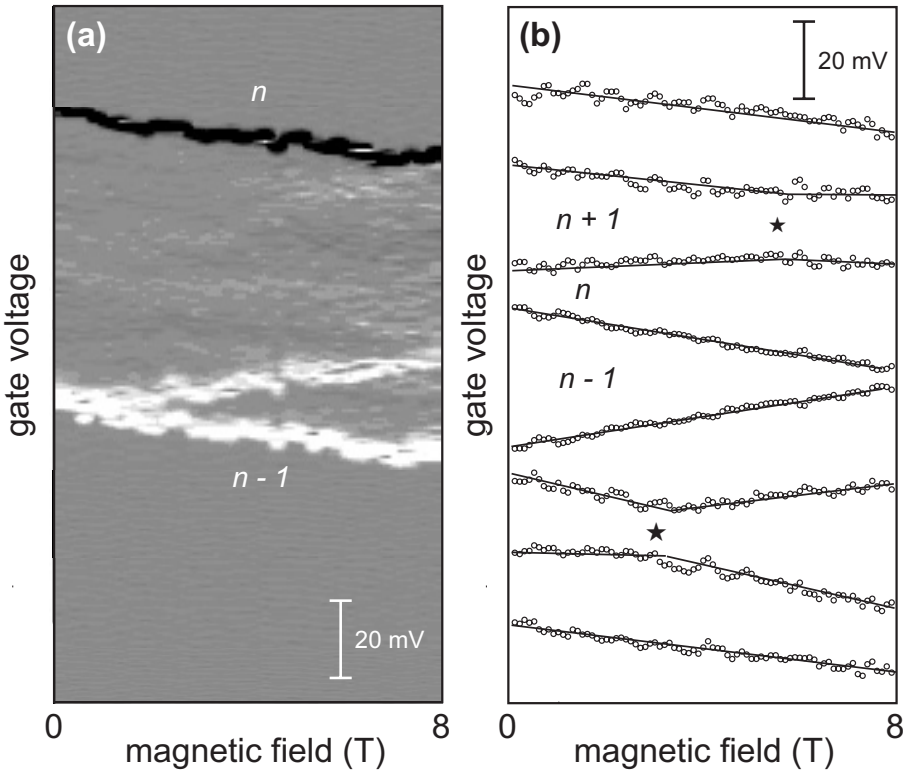

Figure 2.7: Magnetoconductance measurement on a nanotube. **a**) Current through the nanotube at $V_{bias} = 2.5$ mV on the transition from $n-1$ to n as a function of gate voltage. Shown is dI/dV_{gate}, where white (black) corresponds to positive (negative) values. The low gate voltage ground state splits in two as the magnetic field is increased from 0 to 8 T. This splitting is linear and yields a Landé g_L-factor of 1.9 ± 0.2. **b**) Zero-bias voltage conductance peak position as a function of magnetic field. The curves are shifted along the gate voltage axis for clarity. The solid lines are guides to the eye. The stars ($\star$) indicate kinks in adjacent lines.

i.e. the transition from n to $n+1$. The shifting of this conductance peak in Fig. 2.7b, however, appears quite different. Measurements on other transitions yield similar discrepancies between excitation and addition spectrum regarding the spin-degree of freedom.

It appears that this spin degeneracy is visible in the excitation spectrum, but not in the addition spectrum in $B = 0$ T. Recently, it has been shown that the transport properties of nanotubes can be interpreted in terms of the Luttinger liquid model (see [13, 17] and chapters 3, 5, and 6), in which spin and charge are separated. This spin-charge separation turns the spin degree of freedom into a neutral collective excitation. We hope that the present studies will encourage

theoretical studies on the role of spin-charge separation on the addition and excitation spectra of carbon nanotubes. The first excitation spectra have been theoretically studied already for carbon nanotubes [14]. The predicted structure, however, is too simple to account for the structure in the present data.

In a nanotube, a pattern of either peaks going up, down, etc. or up, up, down, down, etc. is expected, depending on whether the two sets of energy levels are degenerate or not. This pattern is not present. In a previous experiment, it was found that all conductance peaks go down in gate voltage with increasing magnetic field [6]. This pattern is also not present.

Very recently the effect of a non-uniform gate potential profile on spin-flip scattering has been studied theoretically [18]. In this study, the particular potential profile gives rise to various internal spin flip processes, leading to a counter-intuitive shifting of the ground state with magnetic field. This may provide an interesting starting point to explain our data, but further research is needed to experimentally address these issues in a controlled way.

Two positions in Fig. 2.7a, marked by stars ($\star$), show changes in the trend of the peak position versus magnetic field. In the simplest model, this can be explained as follows. When the ground state and the first excited state both split with magnetic field, this splitting is equal to $g_L \mu_B B/\alpha$. When this splitting becomes equal to the level-spacing ΔE, the energy-levels of the excited state with up spin (or down) and the ground state with down spin (or up) cross. This crossing then gives rise to kinks in the peak-position versus magnetic field [6]. From the condition $\Delta E_n = g_L \mu_B B/\alpha$, $g_L = 2$ and the values for ΔE_n from Fig. 2.6, we find magnetic fields larger than 10 T where these crossings may occur. This simple model of crossing can clearly not explain the present data. This may be due to e.g. electrostatic repulsion between the energy levels, i.e. exchange interaction.

Summing up, while some features in the spectra can be understood from available models, the general conclusion is that the excitation and addition spectra, and their relation, are very complex and not well understood.

4 Conclusions

We have observed resonant tunneling through single molecular levels in a carbon nanotube. The obtained addition and excitation spectra in zero magnetic field are

linearly correlated. In a magnetoconductance measurement, Zeeman splitting of the molecular levels has been observed. The filling of single particle levels appears not to behave as expected from simple models. Internal spin-flip processes and interaction mechanisms may be important.

Acknowledgements

The nanotube material is supplied by Richard Smalley and coworkers at Rice University, USA. We would like to thank Leo Kouwenhoven for stimulating discussions. This research was supported by the Dutch Foundation for Fundamental Research of Matter (FOM).

This chapter has been published in J. Low Temp. Phys. **118**, 495 (2000).

References

[1] C. Dekker, *Physics Today* **52 (5)**, 22 (1999).

[2] M. Bockrath *et al.*, *Science* **275**, 1922 (1997).

[3] S.J. Tans *et al.*, *Nature* **386**, 474 (1997).

[4] D.H. Cobden, M. Bockrath, P.L. McEuen, A.G. Rinzler, and R.E. Smalley, *Phys. Rev. Lett.* **81**, 681 (1998).

[5] C.W.J. Beenakker, *Phys. Rev. B* **44**, 1646 (1991).

[6] S.J. Tans, M.H. Devoret, R.J.A. Groeneveld, and C. Dekker, *Nature* **394**, 761 (1998).

[7] H. Grabert and M. Devoret (eds) in *Single Charge Tunneling* (Plenum, New York, 1992).

[8] L.P. Kouwenhoven and C.M. Marcus and P.L. McEuen and S. Tarucha and R.M. Westerveld and N.S. Wingreen, in *Mesoscopic Electron Transport*, edited by L.L. Sohn and L.P. Kouwenhoven and G. Schon (Kluwer, Dordrecht, The Netherlands.

[9] D.R. Stewart *et al.*, *Science* **278**, 1784 (1997).

[10] A. Thess *et al.*, *Science* **273**, 483 (1996).

[11] S.J. Tans, A.R.M. Verschueren, and C. Dekker, *Nature* **393**, 49 (1998).

[12] H.W.Ch. Postma, A. Sellmeijer, and C. Dekker, *Adv. Mater.* **17**, 1299 (2000).

[13] M. Bockrath *et al.*, *Nature* **397**, 598 (1999).

[14] C.L. Kane, L. Balents, and M.P.A. Fisher, *Phys. Rev. Lett.* **79**, 5086 (1997).

[15] A. Bezryadin, A.R.M. Verschueren, S.J. Tans, and C. Dekker, *Phys. Rev. Lett.* **80**, 4036 (1998).

[16] Note also that either scenario would make our labeling of excited states in figure 2.5 unjustified.

[17] Z. Yao, H.W.Ch. Postma, L. Balents, and C. Dekker, *Nature* **402**, 273 (1999).

[18] Y. Oreg, K. Byczuk, and B.I. Halperin, *Phys. Rev. Lett.* **85**, 365 (2000).

Chapter 3

Carbon nanotube intramolecular junctions

Z. Yao, H.W.Ch. Postma, L. Balents, and C. Dekker

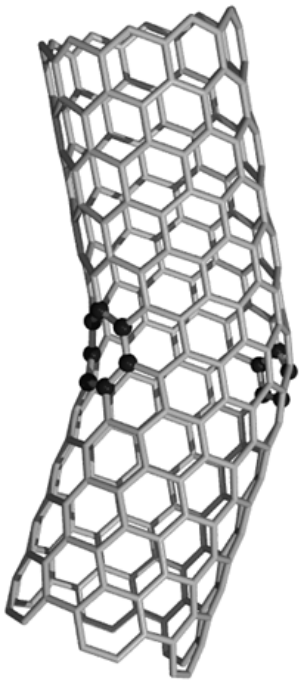

Abstract: The ultimate device miniaturization would be to use individual molecules as functional devices. Single-wall carbon nanotubes are promising candidates for achieving this: depending on their diameter and chirality, they are either one-dimensional metals or semiconductors [1,2]. Single-electron transistors employing metallic nanotubes [3,4] and field-effect transistors employing semiconducting nanotubes [5] have been demonstrated. Intramolecular devices have also been proposed which should display a range of other device functions [6–11]. For example, by introducing a pentagon and a heptagon into the hexagonal carbon lattice, two tube segments with different atomic and electronic structures can be seamlessly fused together to create intramolecular metal-metal, metal-semiconductor, or semiconductor-semiconductor junctions. In this chapter, we report electrical transport measurements on carbon nanotubes with intramolecular junctions. We find that a metal-semiconductor junction behaves like a rectifying diode with nonlinear transport characteristics that are strongly asymmetric with respect to bias polarity. In the case of a metal-metal junction, the conductance appears to be strongly suppressed and it displays a power-law dependence on temperatures and applied voltage, consistent with tunnelling between the ends of two Luttinger liquids. Our results emphasize the need to consider screening and electron interactions when designing and modelling molecular devices. Realization of carbon-based molecular electronics will require future efforts in the controlled production of these intramolecular nanotube junctions.

Figure 3.1a and b display examples of atomic force microscope images of nanotube junction devices. Each nanotube consists of two straight segments, both with measured heights of ~ 1 nm, connected by a sharp kink of about 40°. In principle, such kinks can originate from two different mechanisms: a pentagon-heptagon (5–7) topological defect pair as illustrated in the inset to Fig. 3.1a, or a local mechanical deformation in a uniform nanotube. Both experiments and simulations [13, 14] have shown that a nanotube will elastically deform under a small bending stress, and buckle if the local curvature exceeds a critical value. In this case, a height increase at the buckling point is expected (chapter 4). From our microscope images, however, the kinks appear to be very abrupt, and there seems to be no height increase at the kinks. This suggests that the kinks are due to 5–7 defects. Insertion of a pentagon (or heptagon) into the hexagonal carbon network creates a caplike (or saddlelike) curvature. A 5–7 pair will in general lead to a kink (see inset to Fig. 3.1a). In order to generate a kink of a large

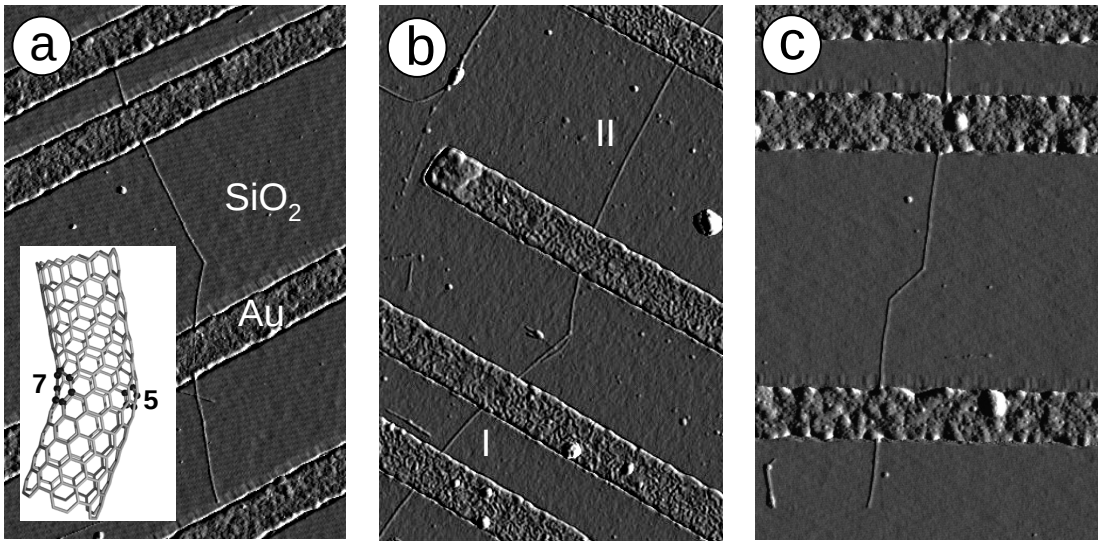

Figure 3.1: Tapping-mode atomic force microscope amplitude images of examples of nanotube junction devices. **a**), **b**), Nanotubes that contain a single kink of 36° and 41° respectively. We have detected in total four single-kink and one double-kink (c) samples out of the $\sim$ 500 devices we have inspected. These kinks can be associated with pentagon and heptagon defects which join two nanotube pieces with different diameters and chiralities. Inset to (a) Illustration of the carbon-bond network of a kink junction constructed between an 'armchair' tube and a 'zigzag' tube, where 5 denotes a pentagon, 7 denotes a heptagon, and the atoms in the pentagon and heptagon are highlighted by dark balls. The nanotube in (a) is on top of three electrodes. Device (b), with four leads connected, represents the ideal geometry, where both straight segments, I and II, and the kink can be characterized separately. The 250-nm wide, 20-nm-thick titanium-gold electrodes are embedded in SiO_2 with a height difference of less than 1 nm, which minimizes the deformation of the nanotubes. This is achieved by standard electron-beam lithography, evaporation and lift-off, combined with an additional step of reactive-ion etching. A highly-doped silicon substrate below SiO_2 is used as a gate to vary the carrier density of the nanotubes. Nanotubes are deposited on top of the electrodes by spin coating of a drop of nanotube suspension in dichloroethane. The two-terminal resistance of an individual straight metallic nanotube is typically ≤ 100 kΩ at room temperature [12], more than an order of magnitude less than in earlier experiments [3, 5]. The low tube-electrode contact resistance proves essential in this work.

angle, the pentagon and heptagon must be placed on the opposite sides of the kink [7]. Further structural evidence for the occurrence of 5–7 pairs comes from a double-kink sample shown in Fig. 3.1c.

The nanotube shown in Fig. 3.1a is lying on three electrodes. The upper straight segment has a two-terminal linear resistance of 110 kΩ at room temperature (inset to Fig. 3.2a) with no gate-voltage dependence, indicating that it is metallic [5]. In striking contrast, the current-voltage ($I-V$) characteristic across the kink (shown in Fig. 3.2a) is highly nonlinear and asymmetric, resembling that of a rectifying diode. The current rises sharply above a threshold voltage for a positive bias applied to the upper electrode. There is a small increase in current for large reverse bias. Around zero bias, the junction impedance is immeasurably high. Rectifying behavior as a possible signature for metal-semiconductor (M–S) heterojunctions was previously observed in a film of entangled nanotubes [15]. However, the junctions were not explicitly observed, and contact with metal electrodes and intertube tunnelling, which can also give rise to the observed behavior, cannot be excluded. The $I-V$ characteristics presented here are clearly associated with the kink defect. We have also measured $I-V$ characteristics for different gate voltages V_g (Fig. 3.2b). The $I-V$ curve seems to shift along the bias voltage axis as a function of V_g (inset to Fig. 3.2b). Upon application of a negative V_g, the $I-V$ curve becomes increasingly asymmetric. The curve at $V_g = -4$ V shows almost perfect rectifying behavior up to the largest bias voltage (-4 V) that we have applied. The strong gate modulation demonstrates unambiguously that the lower nanotube segment is semiconducting and that the kink is an M–S heterojunction.

For an isolated nanotube containing an M–S junction, the Fermi energy of the metallic segment is aligned with the middle of the energy gap of the semiconducting segment. The alignment is modified when the sample is connected to metal electrodes. Owing to the higher work function for the metal, both pieces will be hole-doped by the electrodes [1,5]. The difference in electronic structures and screening properties of metallic and semiconducting nanotubes will give rise to different band-bending profiles in the tube segments away from the electrodes and subsequently a Schottky-type barrier at the M–S interface, which may explain the rectifying behavior across the junction. Further modelling is required to understand the details of the $I-V$ characteristics.

Each of the two straight segments of the sample in Fig. 3.1b lies on two electrodes, which permits their separate characterization and also two- and four-

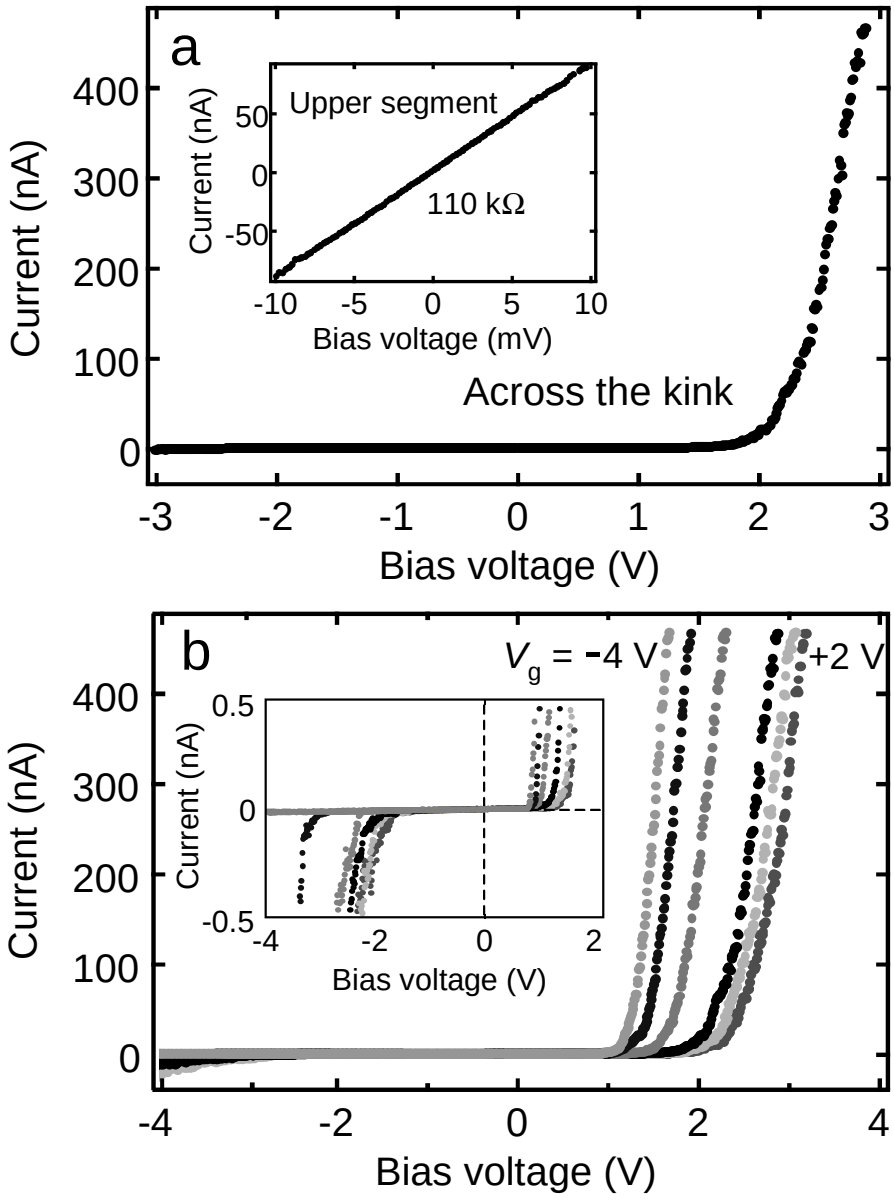

Figure 3.2: Current-voltage characteristics across the metal-semiconductor junction of Fig. 3.1a, showing rectifying behavior. The data are taken at 100 K. The results at room temperature are similar, but the data are noisier. Inset to (a), the $I-V$ curve for the upper straight segment measured at room temperature. The low resistance value and the absence of a gate effect indicate that this segment is metallic. In (a), the gate is grounded. In (b), the gate voltages from right to left are 2 V, 1 V, 0 V, −1 V, −2 V and −4 V respectively. Inset to (b), expanded view of the small-current region which shows more clearly the onset of conduction for both bias polarities. The junction resistance around zero bias is > 250 GΩ. The strong gate modulation demonstrates convincingly that the kink is a metal-semiconductor heterojunction.

terminal measurements across the kink. Figure 3.3 shows the temperature (T) dependence of the two-terminal conductance (G) measured between different electrodes at zero bias. At room temperature, the resistances of the two straight segments are 56 and 101 kΩ respectively, with no gate-voltage dependence, demonstrating that both are metallic. The resistance across the junction is 608 kΩ, which is much higher. As the temperature decreases, all the conductances decrease monotonically. The conductance across the junction depends much more on temperature than that of the two straight segments, and decreases over one order of magnitude as the temperature decreases from 300 K to 50 K. Four-terminal and two-terminal measurements across the kink give essentially the same conductance value, indicating that the observed temperature dependence is completely dominated by the junction itself.

Although a defect is always expected to degrade the conductance, simple tight-binding calculations, which neglect electron-electron interactions, of the conductance across a metal-metal (M–M) kink junction cannot produce the large suppression seen in our experiments [18]. In Fig. 3.3 the data are plotted on a double-logarithmic scale. It appears that all the conductances can be fitted with a power-law function of T, $G \propto T^{\alpha}$, which is particularly convincing for the conductance across the junction because of its strong temperature dependence. Power-law behavior of G versus T was reported recently for metallic ropes of nanotubes [16], and was interpreted as a signature for electron-electron correlations [19, 20]. It has been known for decades that electron interactions are of great importance in one-dimensional transport [21]. Electrons form a correlated ground state called Luttinger liquid (LL), in which the tunnelling density of states is suppressed as a power-law function of energy, $\rho(E) \propto E^{\alpha}$. Tunnelling into the end of an LL is more strongly suppressed than into the bulk, that is, the exponent for end tunnelling α_{end} is larger than the exponent for bulk tunnelling α_{bulk}. For an LL connected to three-dimensional reservoirs by tunnel barriers, the tunnelling conductance in the linear-response regime should vary as $G(T) \propto T^{\alpha}$ (for $eV \ll k_B T$, where e is the electron charge and k_B is the Boltzmann constant) and the differential conductance dI/dV at large bias ($eV \gg k_B T$) should vary as $dI/dV \propto V^{\alpha}$. An interesting question arises when a tunnel junction is placed between two LLs [21]. To a first-order approximation, the tunnelling conductance across the junction is proportional to the product of the end-tunnelling density of states on both sides and therefore still varies as a power law of energy, but with an exponent twice as large as the end tunnelling exponent, that is, $\alpha_{end-end} = 2\alpha_{end}$.

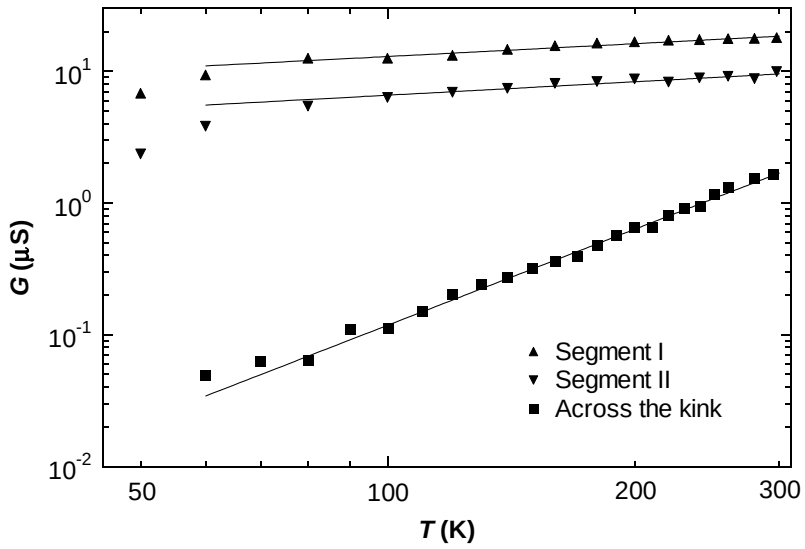

Figure 3.3: Linear-response two-terminal conductances G of segments I and II and across the metal-metal junction of Fig. 3.1b, plotted versus temperature T on a double-logarithmic scale. The data are fitted (solid lines) by the power law, $G(T) \propto T^{\alpha}$, which is associated with the suppression of tunnelling density of states in a Luttinger liquid. The exponents α for the two straight segments are 0.34 and 0.35 respectively. The fit is particularly convincing for the data across the kink. An exponent of 2.2 is obtained, which is consistent with end-to-end tunnelling between two Luttinger liquids. A thermally activated form for transport over a tunnel junction of barrier height U, $G \propto \exp(-U/k_BT)$, does not fit well. For the two straight segments, the overall behavior is similar to that reported for ropes of nanotubes [16], and is typical for our samples of individual nanotubes with similar conductance values (see [17] and chapter 5). The low-temperature deviation from the power law is due to the Coulomb-blockade effect, which sets in when k_BT becomes comparable to the energy e^2/C, needed to put an extra electron onto the nanotube, where C is the total capacitance of the tube (e.g. see chapter 2).

Single-wall carbon nanotubes are truly one-dimensional conductors and are thus expected to behave as LLs. The strength of electron interactions is described by the so-called Luttinger parameter g. For non-interacting electrons $g = 1$, whereas for repulsive Coulomb interactions $g < 1$. The exponents α for tunnelling into the bulk and end of a nanotube are related to g as $\alpha_{bulk} = (1/g + g - 2)/8$ and $\alpha_{end} = (1/g - 1)/4$ respectively [20]. In our experiments, bulk tunnelling is expected for the measurements of the straight segments. Fitting the high-temperature data for the two straight segments yields similar exponents $\alpha =$

0.34 and 0.35, which gives a value of $g \approx 0.22$ using the above expression for bulk tunnelling. This g value agrees with theoretical estimates [19, 20] and with that reported for ropes [16] and clearly indicates the strong electron-electron interactions in carbon nanotubes. Having established that both straight segments are LLs, we expect that the conduction process between the middle two contacts takes place via end-to-end tunnelling between the two LLs as well as tunnelling in and out of the two LLs through the contacts. However, the end-to-end tunnelling dominates the energy dependence of the process. Substituting the above g value into $\alpha_{end-end} = (1/g - 1)/2$, an exponent of 1.8 is expected for the tunnelling conductance across the junction. Fitting the experimental data with a power law yields $\alpha = 2.2$, which is indeed close to this value. This analysis is not based on any presumed g value (which is sample-dependent). The self-consistency of bulk and end-to-end tunnelling thus provides strong evidence for the Luttinger model.

We have also measured large-bias $I - V$ characteristics across the M–M junction at different temperatures, which provide an independent verification of the LL theory. As is evident from Fig. 3.4a, the $I - V$ curves are nonlinear at all temperatures. The current is expected to increase as $V^{\alpha+1}$ for $eV \gg k_B T$. We consider the differential conductance which, assuming a constant tunnelling amplitude across the junction, is predicted to satisfy a scaling function:

$$\begin{aligned} \frac{dI}{dV} &\propto T^{\alpha} \sinh\left(\frac{eV}{2k_BT}\right) \left|\Gamma\left(1 + \frac{\alpha}{2} + i\frac{eV}{2\pi k_BT}\right)\right|^2 \\ &\times \left\{\frac{1}{2}\coth\left(\frac{eV}{2k_BT}\right) - \frac{1}{\pi}\mathrm{Im}\left[\Psi\left(1 + \frac{\alpha}{2} + i\frac{eV}{2\pi k_BT}\right)\right]\right\} \end{aligned}$$

Here α is the end-to-end tunnelling exponent and Γ and Ψ are the gamma and digamma functions respectively. For $\alpha = 2$, a good approximation (exact when $\alpha = 2$) of the above expression is given by $dI/dV \propto T^{\alpha}\,(1 + 3(eV/2\pi k_BT)^{\alpha})$, which clearly shows the expected power-law behavior at large bias. The expression suggests that if we scale dI/dV by T^{α} and V by T, then curves obtained at different temperatures should all collapse onto one universal curve. This is shown in Fig. 3.4b for our experimental data. The scaled conductance is constant for small V but crosses over to a power law for $eV/k_BT > 3$. Its behavior is qualitatively similar to the theoretical scaling function (dashed line) in Fig. 3.4b. The deviation at large bias may be explained by a reduced voltage drop and/or a reduced tunnelling amplitude across the kink (see Fig. 3.4 legend). Overall, however, end-to-end tunnelling between two LLs seems to capture the main physics of the observed data.

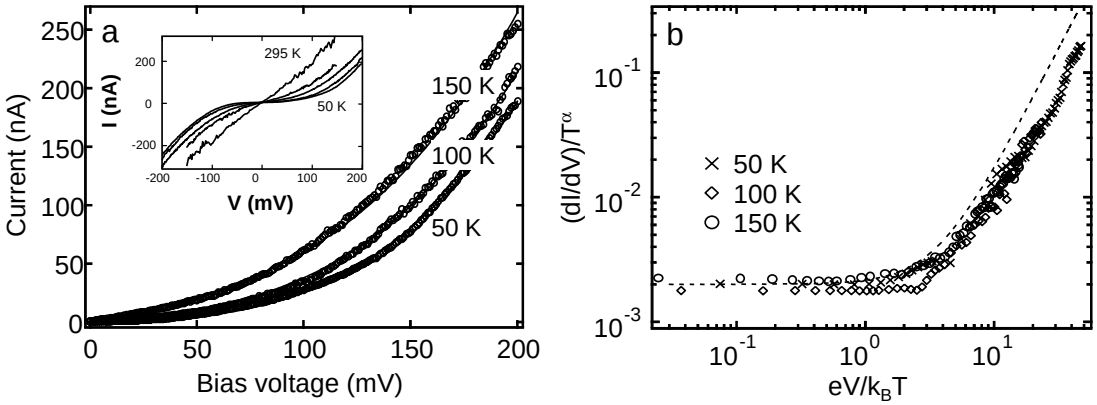

Figure 3.4: Large-bias transport characteristics measured across the metal-metal junction of Fig. 3.1b. **a**) Nonlinear $I-V$ characteristics at different temperatures showing consistency with the Luttinger model. The data are fitted (solid lines) by a phenomenological functional form $I = C_1 T^{\alpha} V\,(1 + C_2(eV/k_BT)^{\alpha})$, where C_1 and C_2 are constants. An exponent of $\alpha = 2.1$ is obtained which is similar to the value from G versus T measurement across the kink. The inset shows $I-V$ curves at temperatures of 298 K, 200 K, 150 K, 100 K and 50 K. **b**) Scaled differential conductance $(dI/dV)/T^{\alpha}$ across the junction plotted against eV/k_BT, where $\alpha = 2.2$ is obtained from the power-law fit of G versus T across the kink. The data taken at various temperatures appear to collapse onto one curve. dI/dV is obtained by numerically differentiating the $I-V$ curves shown in (a). The dashed line represents the theoretical scaling function expected for the end-to-end tunnelling between two Luttinger liquids. At large bias, the measured conductance is lower than the theoretical prediction. Several factors may be responsible for the deviation. We have assumed that the voltage applied between the two contacts drops entirely across the junction, which is reasonable at small bias. As bias voltage is increased, however, more and more voltage drop will occur at the contacts because tunnelling conductance across the contacts (bulk tunnelling) increases less strongly as a function of voltage than that across the junction (end-to-end tunnelling). This effectively leads to reduced conductance across the junction compared to the case where one assumes a complete voltage drop across the junction. Additionally, the tunnelling amplitude across the junction may be energy-dependent at large bias. If the junction is viewed as a nanometer-sized capacitor, charging it to a few hundred millivolts may lead to a strong electrostatic force which could possibly deform the junction and reduce the transmission.

Acknowledgements

We thank R.E. Smalley and co-workers for providing the indispensable single-wall carbon nanotube materials, M.P. Anantram, S.J. Tans and A.A. Odintsov

for helpful discussions, V. Meunier for the atomic coordinates used in the inset to Fig. 3.1a, and M. de Jonge and A. van den Enden for experimental assistance. The work was supported by the Dutch Foundation for Fundamental Research on Matter (FOM).

This chapter has been published in Nature **273**, 402 (1999).

References

[1] J.W.G. Wildoër *et al.*, *Nature* **391**, 59 (1998).

[2] T.W. Odom, J. Huang, P. Kim, and C.M. Lieber, *Nature* **391**, 62 (1998).

[3] S.J. Tans *et al.*, *Nature* **386**, 474 (1997).

[4] M. Bockrath *et al.*, *Science* **275**, 1922 (1997).

[5] S.J. Tans, A.R.M. Verschueren, and C. Dekker, *Nature* **393**, 49 (1998).

[6] L. Chico, V.H. Crespi, L.X. Benedict, S.G. Louie, and M.L. Cohen, *Phys. Rev. Lett.* **76**, 971 (1996).

[7] Ph. Lambin, A. Fonseca, J.P. Vigneron, J.B. Nagy, and A.A. Lucas, *Chem. Phys. Lett.* **245**, 85 (1995).

[8] R. Saito, G. Dresselhaus, and M.S. Dresselhaus, *Phys. Rev. B* **53**, 2044 (1996).

[9] J.-C. Charlier, T.W. Ebbesen, and Ph. Lambin, *Phys. Rev. B* **53**, 11108 (1996).

[10] M. Menon and D. Srivastava, *Phys. Rev. Lett.* **79**, 4453 (1997).

[11] L. Chico, M.P. López Sancho, and M.C. Munoz, *Phys. Rev. Lett.* **81**, 1278 (1998).

[12] Z. Yao, C.L. Kane, and C. Dekker, *Phys. Rev. Lett.* **84**, 2941 (2000).

[13] S. Iijima, C. Brabec, A. Maiti, and J. Bernholc, *J. Chem. Phys.* **104**, 2089 (1996).

[14] B.I. Yakobsen, C.J. Brabec, and J. Bernholc, *Phys. Rev. Lett.* **76**, 2511 (1996).

[15] P.G. Collins, A. Zettl, H. Bando, A. Thess, and R.E. Smalley, *Science* **278**, 100 (1997).

[16] M. Bockrath *et al.*, *Nature* **397**, 598 (1999).

[17] H.W.Ch. Postma, M. de Jonge, Z. Yao, and C. Dekker, *Phys. Rev. B* **62**, R10653 (2000).

[18] L. Chico, L.X. Benedict, D.G. Louie, and M.L. Cohen, *Phys. Rev. B* **54**, 2600 (1996).

[19] R. Egger and A.O. Gogolin, *Phys. Rev. Lett.* **79**, 5082 (1997).

[20] C.L. Kane, L. Balents, and M.P.A. Fisher, *Phys. Rev. Lett.* **79**, 5086 (1997).

[21] M.P.A. Fisher & L.I. Glazman. in *Mesoscopic Electron Transport* (eds L.P. Kouwenhoven, L.L. Sohn, & G. Schön) 331-373 (Kluwer Academic, Boston, 1997).

Chapter 4

Manipulation and imaging of carbon nanotubes with an atomic force microscope

H.W.Ch. Postma, A. Sellmeijer, and C. Dekker

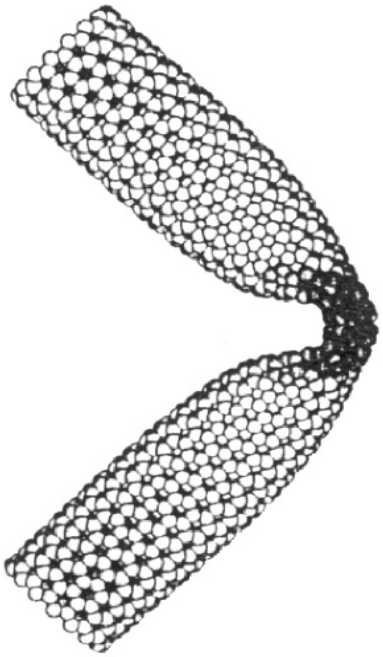

Abstract: The tip of an atomic force microscope is used to create carbon nanotube junctions by changing the position and shape of individual single-wall carbon nanotubes on a SiO_2 surface. With this manipulation technique, we are able to bend, buckle, cross, and break nanotubes, and to unravel a nanotube 'crop circle' into a single tube. Tapping-mode AFM measurements of the height of a carbon nanotube on the surface always yield values smaller than the nanotube diameter. Variation of the scan parameters shows that this is due to a tapping deformation by the tip. The tapping deformation of manipulated nanotube crossings and buckles is discussed as well.

Carbon nanotubes [1] have attracted a lot of interest because of their unprecedented electronic and mechanical properties on a molecular scale (for a review, see e.g. [2]). The interplay of these properties, for example, the effect of mechanical deformations on the electron transport properties, seems to be of particular interest [3–8]. While AFM manipulation experiments have been reported on multi-wall nanotubes [3–5], the prototype single-wall tubes are much more difficult to study since their diameter is more than an order of magnitude smaller. In this chapter, we explore the mechanical properties of individual single-wall carbon nanotubes and nanotube junctions by atomic force microscopy (AFM). We present manipulation experiments on individual single-wall carbon nanotubes, where the tip of an AFM is used to change the nanotube position and shape on a SiO_2 substrate. We show examples where we have used this manipulation technique to locally bend, buckle, break, and cross nanotubes, and where we have unraveled a nanotube 'crop circle' [9]. We also present tapping-mode AFM measurements of the apparent height as a function of the feedback parameters. These measurements show that in typical AFM imaging, nanotubes always appear lower than expected, due to a local and reversible compression of the nanotube by the tapping tip. Height measurements of manipulated buckles and manipulated crossings show that they are slightly more rigid than non-manipulated, individual tubes.

In tapping-mode AFM, a stiff cantilever with a sharp tip attached to the end is oscillated near its resonant frequency resulting in an oscillation amplitude in free air in the range of 1 to 10 nm. When this tip is brought into contact with a sample surface, the amplitude of oscillation is reduced. While scanning the surface, the amplitude of the cantilever oscillation will change whenever a change in the height of the sample surface is encountered. A feedback loop then changes the height of

the cantilever over the surface to maintain a constant setpoint amplitude. Since the tip is only intermittently in contact with the sample, the lateral forces acting on the sample while scanning are negligible. This enables one to image individual single-wall nanotubes lying on a surface without moving them. If, by contrast, the feedback is turned off, the cantilever is pressed down onto the substrate, and dragged along a predefined path over the surface, one can shift the nanotubes laterally. This is the basis of our manipulation technique. We use a commercial AFM mounted with stiff cantilevers with a force constant of about 50 N/m and a resonant frequency of about 300 kHz. The carbon nanotubes, with an average diameter of 1.4 nm, were synthesized by a laser vaporization technique by R.E. Smalley and coworkers at Rice University, USA. They were deposited by spin coating a drop of nanotube suspension on a thermally grown SiO_2 surface. The experiments were performed in air at room temperature.

In Fig. 4.1 we present several intermediate steps of a typical manipulation experiment of a carbon nanotube. The arrows in the image show the path that the AFM tip has travelled in each manipulation step. The initial configuration of a nanotube with an apparent AFM height of 1.8 nm is shown in Fig. 4.1a. The result of the first manipulation step is shown in Fig. 4.1b. The tube has been successfully dragged from its original position and is strongly bent. The tube is held in this strained configuration by attractive van der Waals binding to the substrate. As the tube has shifted sideways, the lower end of the nanotube has been dragged along its original path (indicated by the white line in Fig. 4.1b). Apparently, the nanotube is pinned more strongly at the upper part than at the lower part, consistent with the fact that the upper part is longer and thus experiences a larger binding force. At the original position of the nanotube, traces of debris have become visible. These traces are presumably due to amorphous carbon particles from the suspension of nanotubes. The height of the manipulated piece of nanotube is 1.2 nm, which indicates that the initially measured height appeared higher due to the amorphous carbon. Figure 4.1c shows an enlarged scan of the strongly bent piece. By pushing the nanotube from the lower side, we make the nanotube fold onto itself, as shown in Fig. 4.1d. The next manipulation involved pushing against the upper side. In Fig. 4.1e it is clearly visible that the nanotube has been broken at the point of the sharp end in Fig. 4.1d, and is now crossing itself. The height of the crossing is discussed below. The image in Fig. 4.1f shows a larger image of the manipulation site. Starting from a single nanotube, we have succeeded in fabricating an intermolecular junction.

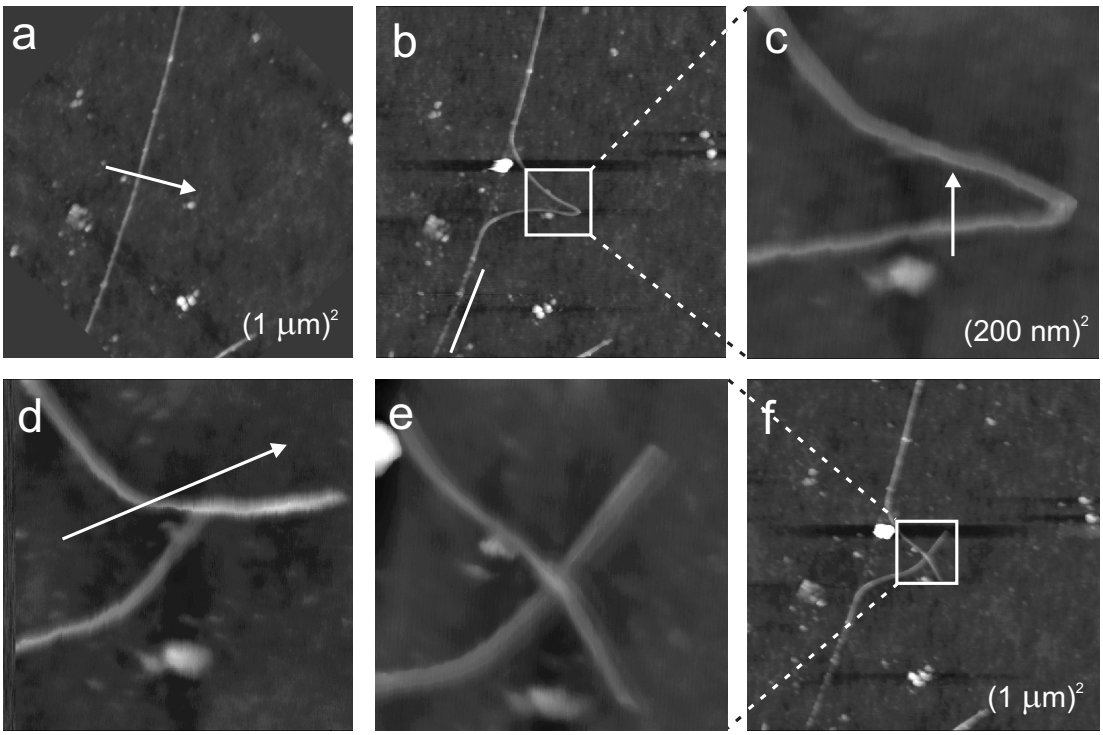

Figure 4.1: Tapping-mode AFM height images of intermediate stages of a typical manipulation experiment. Before each manipulation step, the height profile of the surface is recorded. Then the tip is lowered towards the surface and moved across the surface along a predefined path, indicated in the image with arrows. The nanotube is then imaged again. The sequence (a–f) shows how a nanotube crossing is formed from an individual single-wall nanotube.

Figure 4.2 shows several intermediate stages of the unraveling of a 'fullerene crop circle', a nanotube which is circularly folded onto itself [9]. The initial configuration is shown in Fig. 4.2a. The crop circle has a diameter of 520 nm. Several linear manipulation paths have been used to indent the circle. In Fig. 4.2b the result of these operations shows a nanotube which has been shifted locally while leaving behind a trace of amorphous carbon. The next manipulation step shows the appearance of a single tube (Fig. 4.2c). By pushing the lower right side, we unravel the crop circle to reveal a single tube in Fig. 4.2d. After several further manipulation steps (not shown), the nanotube has been rearranged considerably and has shifted along the surface (Fig. 4.2e). The length of the nanotube in the final configuration is 2.6 ± 0.1 μm, while the height is 0.9 nm. After the discovery of these crop circles, it was discussed whether both ends of the nanotube could

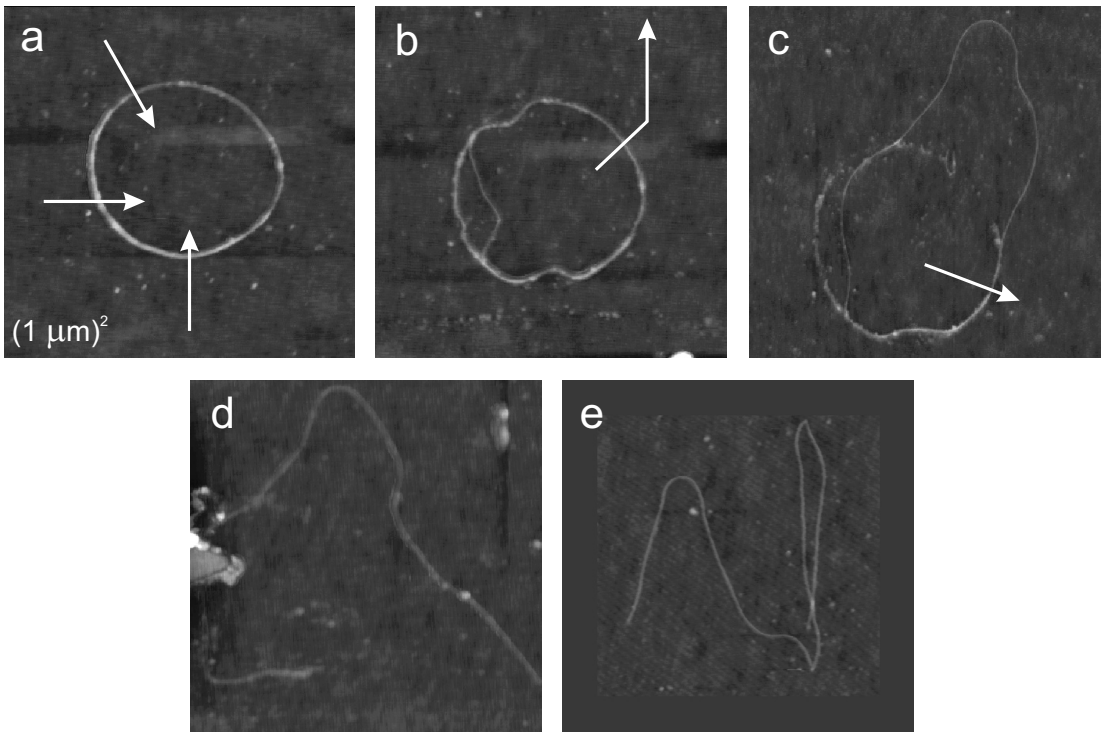

Figure 4.2: Tapping-mode AFM height images of intermediate stages in the unraveling of a fullerene crop circle. The arrows indicate the paths the AFM tip has travelled in each manipulation step. The large structure on the left side of (d) is material which was deposited from the tip onto the substrate during the previous manipulation step. To move the nanotube away from this spot, several manipulation steps (not shown) have been performed, shifting the nanotube to the entire right (e). All images are 1 μm^2.

grow together to form a seamless toroid. We conclude, however, that the crop circle studied here consisted of a single nanotube wrapped almost twice onto itself.

In all of the previous figures, the AFM height of a single nanotube lying on a SiO_2 surface always appears to be lower than expected. Figure 4.3 shows a typical example of height measurements of a nanotube (•) as a function of drive amplitude. The height measurements show values for the apparent height of a nanotube of 0.6 to 1.1 nm, i.e. much smaller than the expected value of 1.7 nm, which is the sum of the nanotube diameter of 1.4 nm and the van der Waals separation between nanotube and surface of about 0.3 nm [10]. The height decreases with increasing drive amplitude. At the highest drive amplitudes, the height appears to level off at a value of 0.6 nm. Note that this is close to the

sum of the graphite interlayer spacing and the separation between nanotube and substrate.

The dependence of the nanotube height, as recorded in tapping-mode AFM, on the drive amplitude can be understood as follows. In free air, the cantilever amplitude is proportional to the drive amplitude. When performing tapping-mode imaging, the cantilever is lowered towards the sample surface to reduce the amplitude to the setpoint value. The degree of reduction is a monotonic function of the average height of the cantilever over the surface. If the drive amplitude is increased, the tip has to be lowered further towards the sample surface in order to maintain the same setpoint amplitude. The necessary tip-height reduction depends on the compressibility of the sample. In our experiments, the SiO_2 surface is much less compressible than the nanotube. The height reduction over the substrate is thus much smaller than over the nanotube. This leads to a decrease of the apparent nanotube height when increasing the drive amplitude due to an inelastic, reversible, and local indentation of the nanotube. This is consistent with the data presented here.

The nanotube crossing presented in Fig. 4.1 has an apparent AFM height of 2.8 nm, whereas the individual nanotube pieces appear to be 1.2 nm high. The expected height of a nanotube crossing consists of twice the nanotube diameter, the spacing between the crossing nanotubes, and the separation between nanotube and substrate. For our nanotubes, this yields an expected crossing height of 3.4 nm. In this crossing configuration, both nanotubes are thus each compressed by 0.3 nm by the tapping tip. The straight segments of the non-manipulated individual nanotube, however, are compressed by 0.5 nm by the tapping tip. This difference is a result of the fact that the nanotubes in the crossing configuration share the tapping deformation. This makes this configuration more rigid than a single tube, leading to a smaller compression of each nanotube at the crossing compared to an individual nanotube. The same effect can be observed in Fig. 4.1d, where the folded piece of tube appears significantly higher than the individual parts. This is a result of the fact that both pieces are lying so close together, that they are indented simultaneously by the tapping tip. Therefore, they share the tapping deformation, leading to a smaller compression and a larger apparent height.

We have also studied the height of manipulated nanotube buckles as a function of the scan parameters. A typical example of such a manipulated buckle is shown in the inset of Fig. 4.3. The buckle has been obtained by AFM manipulation

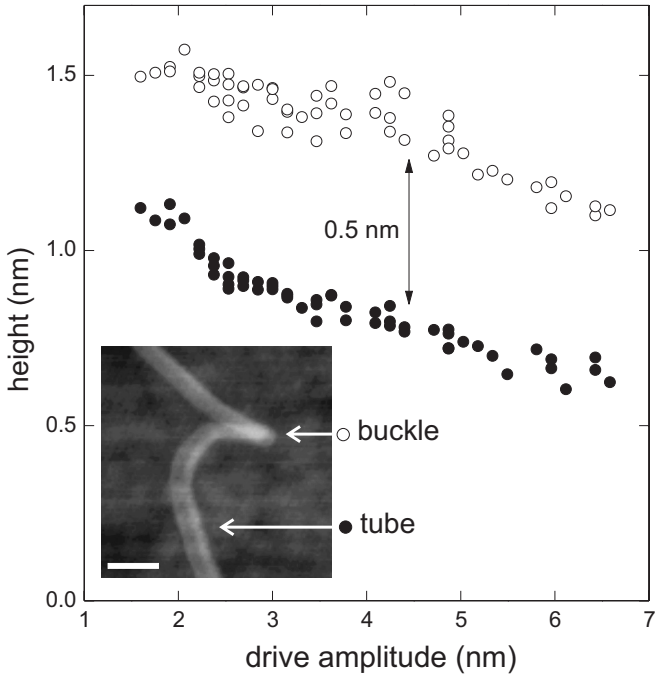

Figure 4.3: Tapping-mode AFM height of a nanotube (•) and a manipulated nanotube buckle (∘) as a function of the drive amplitude for setpoints from 2 to 6 nm. Below this range the feedback of the AFM does not function properly. For these measurements, the nanotube has been shifted lateraly such that the height measurements are not affected by any amorphous carbon traces. The inset shows a height image; the white scale bar is 50 nm.

similar to Fig. 4.1a–c. Buckle formation has been studied before for multi-wall nanotubes [3–5]. In that case, the presence of multiple walls inside the outer shell modifies the characteristics of the buckling, as compared to the theoretical models for single-wall tubes [11]. Here, however, we experimentally study buckling in single-wall nanotubes. The expected degree of bending necessary to form a buckle for the nanotubes used in our experiments is 0.08 rad/nm [11]. From the AFM image, we estimate that the buckle is at least localized within a nanotube length equal to the width of the tip, about 20 nm, and that the angle is π rad. This yields a lower limit for the degree of curvature of about 0.16 rad/nm, which is well above the theoretical minimum. The expected height of a buckle is $\pi/2$ times the diameter of a nanotube, plus the separation between nanotube and substrate. This amounts to 2.5 nm. The measurements presented in Fig. 4.3 (∘) show that the buckle indeed appears higher than a non-manipulated nanotube, by about 0.5 nm. Similar to the case of nonmanipulated tubes, the buckle height of 1.1 to 1.6

nm is again smaller than expected theoretically and it decreases with increasing drive amplitude. The trends of the buckle and nanotube heights as a function of drive amplitude appear very similar, which seems to indicate that the rigidity of buckles and straight nanotubes are similar. However, because the AFM tip is more wide than the nanotube, the area of a single nanotube which is deformed is larger than the area of the buckle, since buckles are higher than straight tubes. We therefore conclude that buckles are more rigid than undeformed nanotubes. This is reasonable, because buckles are not hollow but filled objects. Height measurements on other buckles in air as well as under an atmosphere of N_2 gas show similar behavior.

The present work shows that artificial nanotube junctions can be created by manipulation of individual single-wall nanotubes. The formation of structures such as nanotube buckles, bends, and crossings opens a route towards transport studies of junctions within nanotubes. First transport studies of a naturally occurring crossing of nanotube ropes [7] and nanotube kink junctions (see [8] and chapter 3) show that molecular junctions can indeed have interesting properties. Transport measurements on our manipulated junctions made from individual single-wall nanotubes show a 4-terminal room-temperature resistance of nanotube buckles and crossings of approximately 1 – 10 MΩ, which is much higher than the typical value of order 10 kΩ for non-manipulated nanotubes. A detailed study of the transport characteristics of these junctions is presented in chapter 5 (see also ref. [12]).

Acknowledgements

This research is financially supported by the Dutch Foundation for Fundamental Research on Matter (FOM). We thank Z. Yao for experimental assistance and discussions. The nanotube material was supplied by R.E. Smalley and coworkers at Rice University, USA. The image on page 41 is taken from [11].

This chapter has been published in Adv. Mater. **17**, 1299 (2000).

References

[1] S. Iijima, *Nature* **354**, 56 (1991).

[2] C. Dekker, *Physics Today* **52 (5)**, 22 (1999).

[3] E.W. Wong, P.E. Sheenan, and C.M. Lieber, *Science* **277**, 1971 (1997).

[4] M.R. Falvo *et al.*, *Nature* **389**, 582 (1997).

[5] T. Hertel, R. Martel, and Ph. Avouris, *J. Phys. Chem. B* **102**, 910 (1998).

[6] A. Bezryadin, A.R.M. Verschueren, S.J. Tans, and C. Dekker, *Phys. Rev. Lett.* **80**, 4036 (1998).

[7] J. Lefebvre *et al.*, *Appl. Phys. Lett.* **75**, 3014 (1999).

[8] Z. Yao, H.W.Ch. Postma, L. Balents, and C. Dekker, *Nature* **402**, 273 (1999).

[9] J. Liu *et al.*, *Nature* **385**, 780 (1997).

[10] L.C. Venema, V. Meunier, Ph. Lambin, and C. Dekker, *Phys. Rev. B.* **61**, 2991 (2000).

[11] S. Iijima, C. Brabec, A. Maiti, and J. Bernholc, *J. Chem. Phys.* **104**, 2089 (1996).

[12] H.W.Ch. Postma, M. de Jonge, Z. Yao, and C. Dekker, *Phys. Rev. B* **62**, R10653 (2000).

Chapter 5

Electrical transport through carbon nanotube junctions created by mechanical manipulation

H.W.Ch. Postma, M. de Jonge, Z. Yao, and C. Dekker

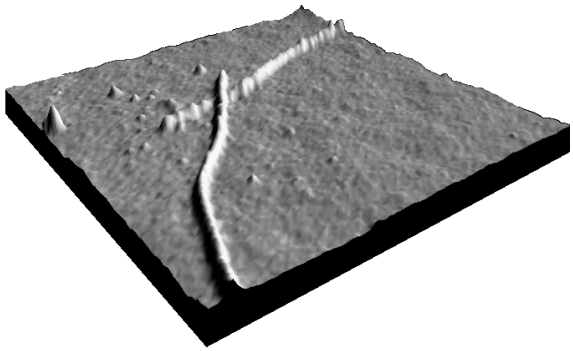

Abstract: Using an atomic force microscope we have created nanotube junctions such as buckles and crossings within individual single-wall metallic carbon nanotubes connected to metallic electrodes. The electronic transport properties of these manipulated structures show that they form electronic tunnel junctions. The conductance shows power-law behavior as a function of bias voltage and temperature, which can be well modeled by a Luttinger liquid model for tunneling between two nanotube segments separated by the manipulated junction.

Molecular electronics has taken a large step forward since the discovery of carbon-nanotube metallic and semiconducting molecular wires [1]. Various nanotube devices have been found to behave as conventional electronic components. For instance, individual semiconducting nanotubes function as field-effect transistors at room temperature [2], while metallic nanotubes are single-electron transistors at low temperature [3, 4]. More recently, it was found that intramolecular metal-semiconductor kink junctions can act as rectifying diodes at room temperature (see [5] and chapter 3). Unlike conventional solid-state devices, however, nanotubes are molecules. Conformational changes can therefore be expected to strongly affect the electronic properties of nanotubes, opening up a route towards nanoscale electro-mechanical devices (NEMs). Indeed, theoretical work has indicated that local deformations such as twists and buckles may induce strong barriers for electron transport [6–8]. While some transport experiments have been conducted on carbon nanotube junctions which occur naturally [5, 9, 10] and on defects due to locally applied strain [11], a focused study with control over the geometry and configuration of the junction is lacking.

In this chapter, we report electron transport measurements on molecular junctions that have been fabricated in a controlled manner from straight undeformed nanotubes by manipulation with an atomic force microscope (AFM). We have fabricated nanotube buckles and crossings and characterized their electron transport properties. We find that these mechanically manipulated structures act as tunnel junctions with a conductance that show power-law dependences on both bias voltage and temperature. For various sample layouts we obtain a wide range of power-law exponents, from 0.25 to 1.4. We show that this variety can be understood within one self-consistent Luttinger model.

Single-wall carbon nanotubes were produced by the group of R.E. Smalley at Rice University, USA. A small amount of this raw material is ultrasonically

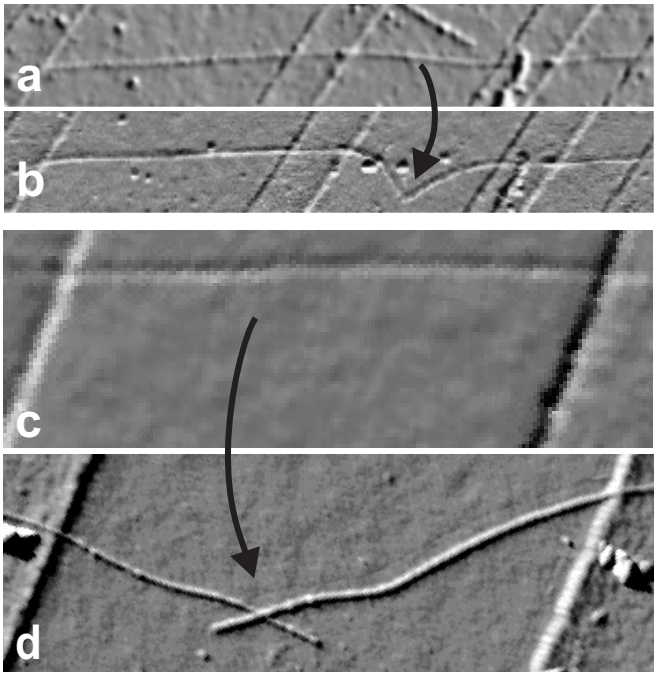

Figure 5.1: Formation of carbon nanotube nanojunctions by AFM manipulation. Between the images in (a) and (b), an initially straight nanotube has been dragged to the bottom by the AFM tip, resulting in a sharp 105° buckle. Image (c) and (d) show the manipulation of a nanotube crossing from an initially straight nanotube. The nanotube ends are extending 110 (left) and 130 nm (right) beyond the crossing point. The difference in apparent width of the nanotubes in these images is due to variation in the AFM tip radius which is different for different tips, and which moreover can change in the manipulation process.

dispersed and spin coated on top of a SiO_2/Si-substrate containing a large array of predefined Pt electrodes. These electrodes are fabricated using a double layer (PMMA/MAA) resist, electron beam lithography, reactive ion etching, Pt evaporation and lift-off [12]. The resulting electrodes are embedded in the SiO_2 substrate such that the height difference between the electrodes and substrate is less than 1 nm. Nanoscale tunnel junctions are then created within individual carbon nanotubes by use of the AFM. Conductance measurements are performed using a standard ac-lockin technique.

Figure 5.1 presents two examples of nanojunctions that were fabricated with an AFM from individual metallic carbon nanotubes. In the fabrication procedure, the tip of the AFM is used to change the lateral position of a nanotube lying on top of metallic electrodes. First, a nanotube is identified by scanning the

tip over the sample in tapping-mode AFM. Then, the tip is pressed onto the surface and moved along a predefined path across the nanotube. In this manner, the position and shape of nanotubes can be controlled with a high degree of accuracy (see [13] and chapter 4). In Fig. 5.1a we show the initial configuration of a straight nanotube lying across four electrodes. In order to bend the tube between the middle two electrodes, the nanotube has been dragged across the surface in a direction perpendicular to its length. During this dragging action, the nanotube has slided along its length across the electrodes. The sharp bend that results from the AFM manipulation has an angle of 105° (see Fig. 5.1b, and also inset to Fig. 5.2). This is well above the critical value of about 60° needed to form a so-called 'buckle' [14], where a strongly bent nanotube releases strain by locally collapsing the cylindrical shell structure into a flattened tube structure. Accordingly, a small height increase is found at the bending point. Another example of a manipulated nanojunction is shown in Fig. 5.1c and d. In this case, the dragging action of the AFM has broken the nanotube. Subsequently, the two broken ends of this nanotube have been pushed back together into a configuration where they cross each other. The resulting nanotube ends extend about 100 nm beyond the crossing point.

Multiterminal contacting of the nanotube allows one to separately measure the contact conductance (from two- and three-terminal measurements) and the intrinsic conductance of the manipulated tube (from a four-terminal measurement). The buckled nanotube sample in Fig. 5.1b has contacts with a low contact conductance, i.e., only 65 nS at room temperature. The intrinsic buckle conductance appears to be about 1 μS at room temperature. This is much lower than the four-terminal conductance value of order 100 μS that we typically find for non-manipulated straight nanotubes in a similar layout. The effect of the buckle on the electron transport is thus quite dramatic. The buckle conductance is also much lower than the quantum conductance unit of $4e^2/h = 154$ μS, which indicates that the buckle acts as a tunnel barrier.

In Fig. 5.2 the conductance G of the buckled segment is plotted versus temperature T on a double-logarithmic scale for both the two- and four-terminal configuration. At high temperatures the data can be fitted with a power-law function $G \propto T^{\alpha}$ (solid lines). Below 120 K, Coulomb blockade sets in which further suppresses the conductance. The power-law exponent α is found to be very different, $\alpha = 0.26$ versus 1.4, for the two- and four-terminal measurements respectively. The intrinsic buckle conductance (four-terminal data) thus appears

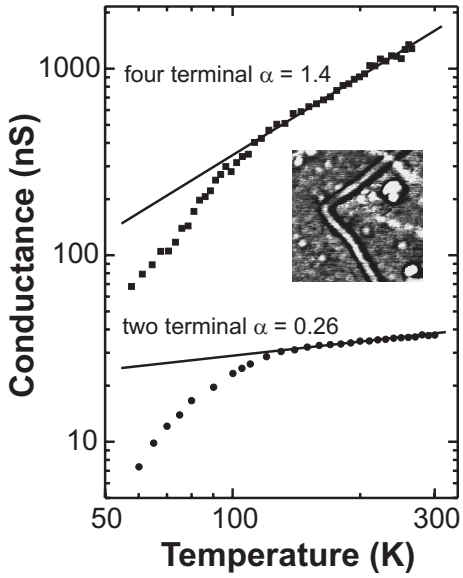

Figure 5.2: Conductance of a nanotube buckle as a function of temperature in a four- and two-terminal measurement. The straight solid lines on this log-log plot indicate the power-law behavior $G \propto T^{\alpha}$, with the exponent α as denoted. Below 120 K, Coulomb blockade sets in which further suppresses the conductance at low temperatures. The inset shows a 300×300 nm^2 AFM phase image of the nanotube buckle. The four-terminal measurement reveals the intrinsic buckle conductance, whereas the two-terminal conductance is limited by the contact conductance.

to be much more strongly temperature dependent than the contact conductance (two-terminal data).

We can understand these findings on the basis of a Luttinger liquid model. The Luttinger model [15, 16] has been employed to explain recent transport experiments on metallic carbon nanotubes [5, 17]. In this model, electron-electron correlations combined with the one-dimensional nature of nanotubes lead to a power-law suppression of the tunneling conductance as a function of energy, $dI/dV \propto E^{\alpha}$. Here E is the maximum of the thermal or voltage energy scale, i.e. k_BT or eV respectively, with k_B Boltzmann's constant and e the electron charge. At low bias voltages $V \ll k_BT/e$ this leads to a power-law behavior of the conductance as a function of T, i.e., $G \propto T^{\alpha}$. At high voltages, however, it yields a power-law dependence on voltage, $dI/dV \propto V^{\alpha}$. The exponent α depends on the strength of the electron-electron interactions which is characterized by the Luttinger interaction parameter g. For repulsive interactions, g ranges from 0 (very strong interactions) to 1 (no interactions). Estimates of

g for carbon nanotubes are in the range of 0.2 – 0.3 [5, 15–17]. The exponent α also depends on the position of tunneling. When electrons are added to the end of the nanotube, the excess electron charge can spread away in one direction only and the tunnel conductance is suppressed strongly with an exponent $\alpha_{end} = (1/g - 1)/4$. Tunneling into the bulk of the nanotube is more weakly suppressed, with $\alpha_{bulk} = (1/g + g - 2)/8$, because the excess charge can now spread in both directions away from the contact.

The conductance of the buckle is suppressed with a power-law exponent $\alpha = 1.4$ (Fig. 5.2). If the buckle acts as a tunnel barrier, transport across the buckle takes place by tunneling of electrons from the end of one nanotube segment to the end of the other segment. This end-to-end tunneling is associated with an exponent twice as large as tunneling into a single end, i.e., $\alpha_{end-end} = 2\alpha_{end} = (1/g - 1)/2$. Solving $\alpha_{end-end} = 1.4$ yields a Luttinger interaction parameter value $g = 0.26$. In the *two*-terminal configuration, however, the contacts limit the conductance and one thus probes bulk tunneling from the contacts to the nanotube. Here we find $\alpha_{bulk} = 0.26$, from which we obtain the *same* Luttinger parameter value $g = 0.26$. It is gratifying that these exponents which are differing by a factor 6, can be reconciled by this single parameter g. The value of $g = 0.26$ is also well in agreement with theoretical estimates [15, 16], recent experiments in a different geometry (see chapter 3 and [5]), and the value of $g = 0.29 \pm 0.04$ that we find for many samples with straight nonmanipulated nanotubes. We thus conclude that the transport characteristics of this buckle are well described by assuming that it acts as an artificially created nanometer-size tunnel junction within an individual nanotube.

We now discuss data for the nanotube-crossing sample shown in Fig. 5.1d. The conductance of the crossing reads 80 nS at room temperature [18]. Again this value is much lower than the conductance quantum indicating that the crossing also acts as a tunnel junction. The conductance again decreases as a power-law upon lowering the temperature, with $\alpha = 0.50$ (not shown). For this sample, the Coulomb blockade effect further suppresses the conductance below 70 K. The bias dependence of the differential conductance at several temperatures is shown in Fig. 5.3. At all temperatures, the data show the same behavior: At low applied bias, dI/dV is constant at a level that scales as a power law with temperature ($\alpha = 0.50$). At high bias voltage it crosses over to a power-law voltage dependence, i.e., $dI/dV \propto V^{\alpha}$ with $\alpha = 0.48$ (dashed line). The dependence of the differential conductance on both energy scales eV and k_BT is emphasized in

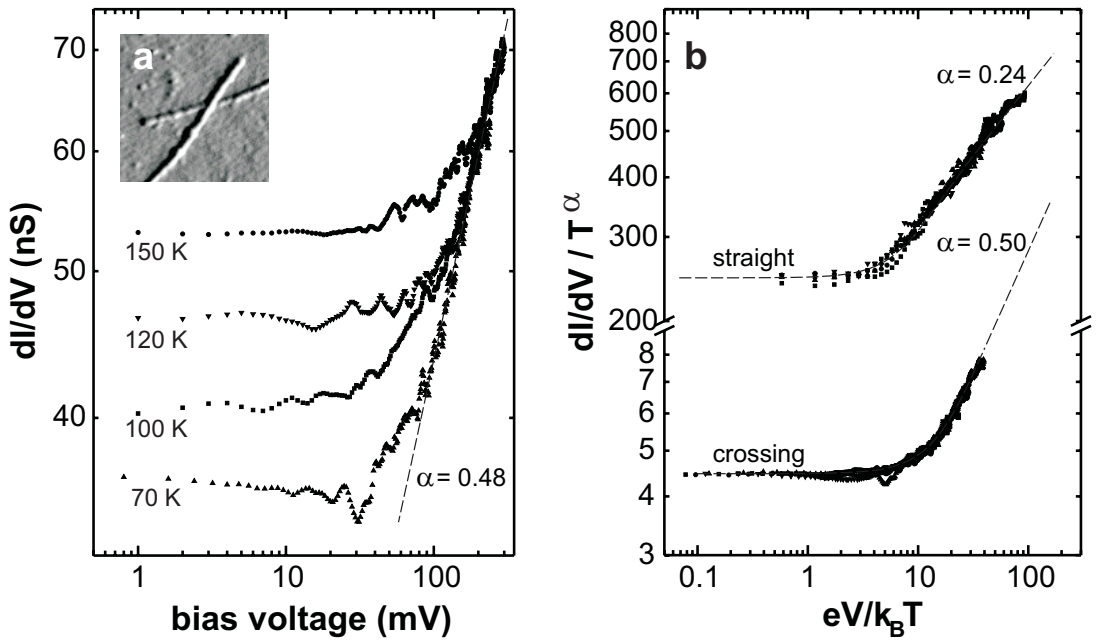

Figure 5.3: **a**) Differential conductance of a manipulated nanotube crossing as a function of applied bias voltage for several temperatures. For this sample, the Coulomb blockade effect suppresses the conductance below 70 K. At low bias voltages, $dI/dV(V)$ is constant while it depends as a power-law on temperature. At high voltages, the differential conductance crosses over to a power-law dependence on bias voltage $dI/dV \propto V^{\alpha}$, with $\alpha = 0.48$ (dashed line). The inset of (a) shows a 200×200 nm^2 AFM amplitude image of the crossing. **b**) Scaling plot, where dI/dV has been scaled by T^{α} and is plotted versus eV/k_BT for the crossing segment and, for comparison, for a typical straight segment of a nanotube.

Fig. 5.3b, where the differential conductance is scaled by T^{α} and plotted versus eV/k_BT. As expected, all the data obtained at different temperatures and bias voltages collapse onto a single curve, which is well described by the theoretically expected form (dashed line) [19]. The exponent α that has been used to scale these curves onto each other is 0.50. Transport between crossing nanotubes was studied recently, but only in the low-bias regime, where this power-law behavior was not observed [10].

The crossing junction thus yields a significantly different value, $\alpha \approx 0.50$, than the buckle junction discussed above. This can be understood as a direct consequence of the particular crossing geometry. Unlike the case for the nanotube buckle where the two tube ends meet, the contact in the crossing is now from

the bulk of one tube to the bulk of the other. The electron transport thus takes place via bulk-to-bulk tunneling [20] with an exponent that is twice as large as that for regular bulk tunneling, i.e., $\alpha_{bulk-bulk} = 2\alpha_{bulk} = (1/g + g - 2)/4$. From $\alpha_{bulk-bulk} = 0.50$ we find $g = 0.27$, which again is in excellent agreement with the other results for g. The bulk-to-bulk tunneling observed for the crossing can be readily compared to the regular bulk-tunneling configuration, which is done in Fig. 5.3b, where the scaled differential conductance is shown for a straight nanotube as well [19]. In this case, the exponent is found to be $\alpha = 0.24$, which indeed is half the exponent observed for bulk-to-bulk tunneling. Molecular dynamics simulations have suggested that crossing nanotubes can be both deformed by about 20% at the crossing point due to the van der Waals binding of the upper nanotube to the substrate away from the crossing [21]. Apparently, this deformation, if present at all, does not electronically break up the nanotubes, since our data indicate that intertube transport occurs via bulk-to-bulk rather than through end-to-end or end-to-bulk tunneling.

Recently, transport experiments were conducted on metal-metal nanotube kink junctions formed by a pentagon-heptagon defect pair located at the kink (see chapter 3 and [5]) and naturally occurring crossing junctions [9,10]. Whereas such junctions are rare objects, the present work shows that one can use an AFM to precisely define local junctions at arbitrary positions along a nanotube. The transport characteristics demonstrate that these local junctions significantly alter the electronic transport properties of carbon nanotubes. A unifying description of single nanotubes, kinks, buckles, and crossings can be obtained from the Luttinger liquid model. The manipulation technique shown here allows the fabrication of various interesting new nanotube structures. For instance, double-buckle structures can be envisioned which define a room-temperature single-electron transistor (see [22,23] and chapter 6). More generally, we expect that electro-mechanical effects may find their use in future nano-electronic devices.

Acknowledgements

We thank A. van den Enden for experimental assistance and L. Balents for useful discussions. The nanotube material was kindly supplied by R.E. Smalley and coworkers at Rice University, USA. This research is financially supported by the Dutch Foundation for Fundamental Research on Matter (FOM) and the European

Community SATURN Project.

This chapter has been published in Phys. Rev. B **62**, R10653 (2000).

References

[1] C. Dekker, *Physics Today* **52 (5)**, 22 (1999).

[2] S.J. Tans, A.R.M. Verschueren, and C. Dekker, *Nature* **393**, 49 (1998).

[3] M. Bockrath *et al.*, *Science* **275**, 1922 (1997).

[4] S.J. Tans *et al.*, *Nature* **386**, 474 (1997).

[5] Z. Yao, H.W.Ch. Postma, L. Balents, and C. Dekker, *Nature* **402**, 273 (1999).

[6] A. Rochefort, D.R. Salahub, and Ph. Avouris, *Chem. Phys. Lett.* **297**, 45 (1998).

[7] C.L. Kane and E.J. Mele, *Phys. Rev. Lett.* **78**, 1932 (1997).

[8] M.B. Nardelli and J. Bernholc, *Phys. Rev. B* **60**, R16338 (1999).

[9] J. Lefebvre *et al.*, *Appl. Phys. Lett.* **75**, 3014 (1999).

[10] M.S. Fuhrer *et al.*, *Science* **288**, 494 (2000).

[11] T.W. Tombler *et al.*, *Nature* **405**, 769 (2000).

[12] Z. Yao, C.L. Kane, and C. Dekker, *Phys. Rev. Lett.* **84**, 2941 (2000).

[13] H.W.Ch. Postma, A. Sellmeijer, and C. Dekker, *Adv. Mater.* **17**, 1299 (2000).

[14] S. Iijima, C. Brabec, A. Maiti, and J. Bernholc, *J. Chem. Phys.* **104**, 2089 (1996).

[15] C.L. Kane, L. Balents, and M.P.A. Fisher, *Phys. Rev. Lett.* **79**, 5086 (1997).

[16] R. Egger and A.O. Gogolin, *Phys. Rev. Lett.* **79**, 5082 (1997).

[17] M. Bockrath *et al.*, *Nature* **397**, 598 (1999).

[18] Initially the crossing nanotube structure was contacted by four electrodes, with the crossing located between the middle two electrodes. The conductance of each of the two middle electrodes were determined to be about 250 nS at room temperature. After the initial measurements, however, the outer contacts were lost, and two-terminal measurements are reported hereafter.

[19] The scaling functions read $(dI/dV)/T^{\alpha} \propto \sinh(\eta x/2)\left|\Gamma\left(1+\alpha/2+i\eta x/2\pi\right)\right|^2 \times \left\{\frac{1}{2}\coth(\eta x/2) - \frac{1}{\pi}\mathrm{Im}\left[\Psi(1+\alpha/2+i\eta x/2\pi)\right]\right\}$ for the bulk-to-bulk tunneling expected for the crossing, and $dI/dV/T^{\alpha} \propto \cosh(\gamma x/2)\left|\Gamma\left(\frac{1+\alpha}{2}+i\gamma x/2\pi\right)\right|^2$ for a straight tube. Here, $x \equiv eV/k_BT$, γ depends on the ratio of the contact conductances, η accounts similarly for the fraction of the applied bias voltage that drops at the contacts to the nanotube, and Γ and Ψ are the gamma and digamma functions, respectively. Using γ and η as fitting parameters, we find $\gamma = 0.6$ and $\eta = 0.18$.

[20] A contact qualifies as a bulk contact if the distance from the contact to the end of the nanotube $L > \hbar v_F/k_BT$, where v_F is the Fermi-velocity and h is Planck's constant [24]. In the sample presented in Fig. 1d, the ends are separated from the crossing point by 110 and 130 nm, which means that all measurements performed at temperatures above 56 K will show bulk-to-bulk tunneling.

[21] T. Hertel, R.E. Walkup, and Ph. Avouris, *Phys. Rev. B* **58**, 13870 (1998).

[22] L. Chico, M.P. López Sancho, and M.C. Munoz, *Phys. Rev. Lett.* **81**, 1278 (1998).

[23] M.S.C. Mazzoni and H. Chacham, *Phys. Rev. B* **61**, 7312 (2000).

[24] L. Balents, cond-mat/9906032. To appear in *XXXIV Moriond Les Arcs Conference Proceedings*, edited by D. C. Glattli and M. Sanquer (Edition Frontiers, France, 1999).

Chapter 6

Carbon nanotube single-electron transistors at room temperature

H.W.Ch. Postma, T.F. Teepen, Z. Yao, M. Grifoni, and C. Dekker

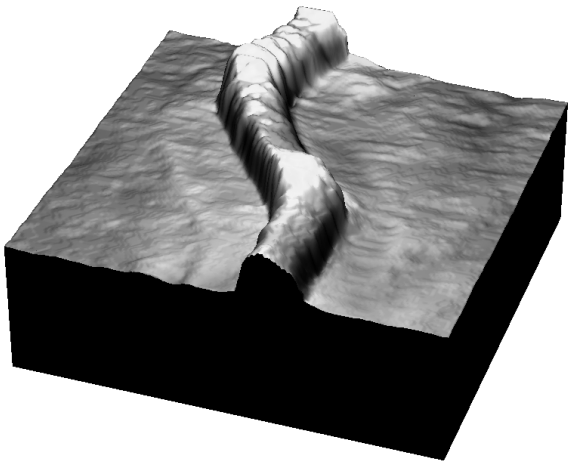

Abstract: Room-temperature single-electron transistors are realized within individual metallic single-wall carbon nanotube molecules. The devices feature a short (down to 20 nm) nanotube section that is created by inducing local barriers into the tube using an atomic force microscope. Coulomb charging is observed at room temperature, with an addition energy of 120 meV which significantly exceeds the thermal energy. At low temperatures, we resolve the quantum energy levels corresponding to the small island. We observe unconventional power-law dependencies in the measured transport properties for which we develop a resonant-tunneling Luttinger-liquid model.

Single-electron transistors (SETs) have been proposed as a future alternative to conventional Si electronic components [1]. Most SETs operate at cryogenic temperatures, however, which strongly limits their practical application. Some examples of SETs with room-temperature operation (RTSETs) have been realized with ultra-small grains, but their properties are extremely hard to control [2–4]. The use of conducting molecules with well-defined dimensions and properties would be a natural solution for RTSETs. In this chapter, we report a first demonstration of room-temperature SETs made within an individual metallic carbon nanotube molecule [5]. We characterize their transport properties as a function of temperature, bias, and gate voltage, and observe unexpected power-law characteristics which we describe with a Luttinger-liquid model.

SETs consist of a conducting island connected by tunnel barriers to two metallic leads [1]. For temperatures and bias voltages low compared to a characteristic energy associated with adding an electron to the island, electrical transport through the device is blocked. Conduction can be restored, however, by tuning a voltage on a close-by gate, rendering this three-terminal device a transistor. In chapter 5, we found that strong bends ('buckles') within metallic carbon nanotubes [5] act as nanometer-size tunnel barriers for electron transport (see also [8]). This motivated us to fabricate single-electron transistors by inducing two buckles in series within an individual metallic single-wall carbon nanotube. This is achieved by manipulation with an atomic force microscope (AFM) (for a detailed description, see chapter 4 and [6]), as displayed in Fig. 6.1. The two buckles define a 25 nm island within a nanotube. We have fabricated a number of these nanotube devices with an island length between 20 and 50 nm, and measured electrical transport through 4 of these. Here we report one representative

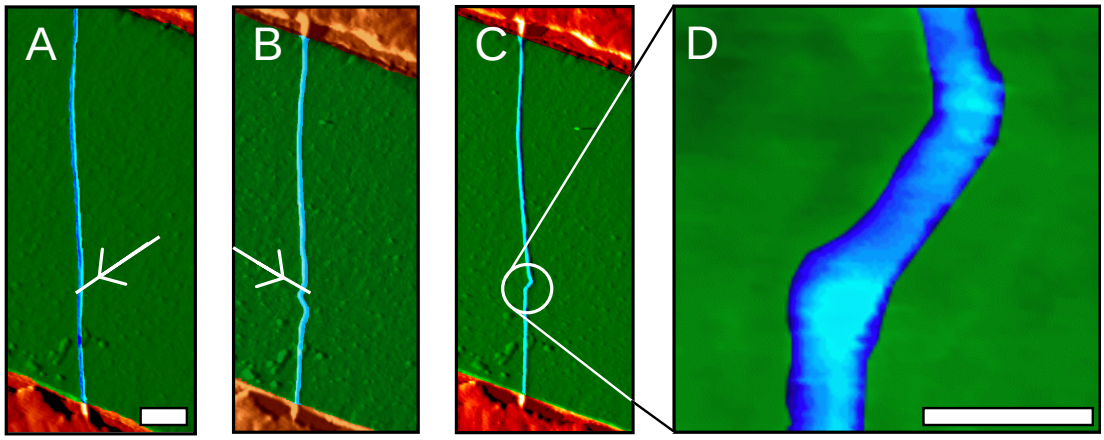

Figure 6.1: Fabrication of a room-temperature single-electron transistors within an individual metallic carbon nanotube by manipulation with an AFM (see chapter 4 and [6]). **a**) Nanotube between Au electrodes on top of a Si/SiO_2 substrate with a gate-independent resistance of 50 kΩ. The scale bar is 200 nm wide. After imaging by scanning the AFM tip over the sample in tapping mode, the tip is pressed down onto the substrate and moved along the path indicated by the arrow, thus dragging the nanotube into a new configuration. **b**) Nanotube after creation of a buckle. The dragging action has resulted in a tube that is bent so strongly that it has buckled [7]. A second dragging action is now performed as indicated by the arrow. **c**) Double-buckle nanotube device. **d**) Enlarged image of the double-buckle device. The scale bar is 20 nm wide. This height image shows a height increase at the buckling points as expected [7]. The final device resistance at room temperature is one order of magnitude larger ($\sim$ 0.5 MΩ). The electronic transport properties of these nanotube devices are studied by application of a bias voltage V to the upper electrode and a measurement of the current I at the lower electrode. The differential conductance dI/dV is measured using a standard ac-lockin technique with a modulation amplitude of 0.1 mV. The conducting Si substrate underneath the insulating SiO_2 substrate is coupled capacitively to the nanotube and acts as a back gate.

data set obtained on the sample with a 25 nm island.

Typical RTSET transport characteristics for our nanotube devices obtained at room temperature are shown in Fig. 6.2a, where the differential conductance dI/dV is plotted versus bias voltage V. A voltage applied to the back gate appears to have a significant effect on the device conductance. A 0.2 V wide gap is observed, which is closed upon changing the gate voltage. Upon varying the gate voltage further, the gap opens and closes in a periodic fashion. At $V = 0$,

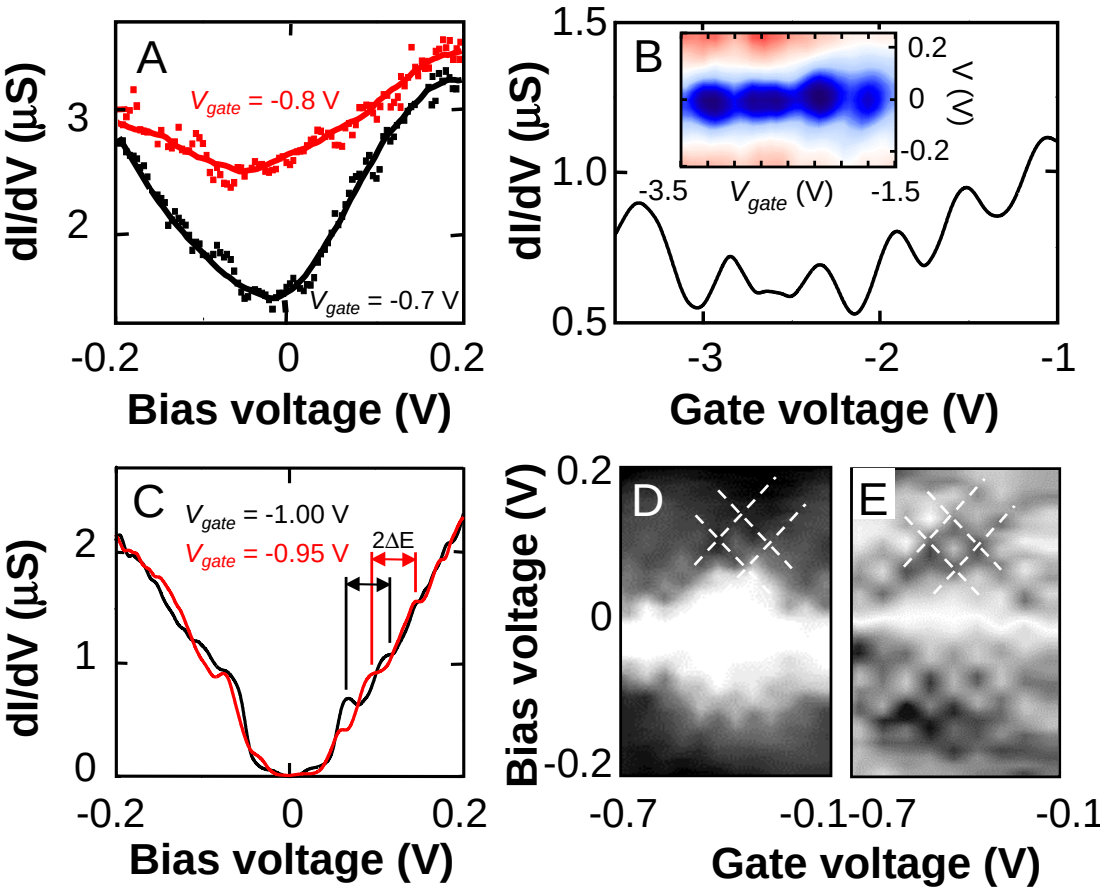

Figure 6.2: Differential conductance dI/dV of the RTSET as a function of bias and gate voltage for several temperatures. **a**) At 300 K, the differential conductance shows a thermally smeared gap around $V = 0$ with gate voltage $V_{gate} = -0.7$ V (lower trace). When the gate voltage is changed to -0.8 V, the gap is closed. **b**) Conductance oscillations as a function of gate voltage at 260 K. The insets shows dI/dV in an intensity plot. Blue represents low dI/dV, red corresponds to high dI/dV. The gap is periodically opened and closed as a function of gate voltage, which results in diamond shaped modulations. **c**) dI/dV at 30 K, showing distinct peaks as indicated by the lines. The peaks in the black trace at $V_{gate} = -1$ V shift up in bias voltage upon increasing V_{gate} to -0.95 V (red trace). **d**) Grey-scale image of dI/dV, where shifting peaks are indicated by the dashed lines. White represents $dI/dV = 0$, while darker shading correspond to higher values of dI/dV. **e**) Grey-scale image of d^2I/dV^2 clarifying the presence of conductance peaks.

this gives rise to a pattern of periodic conductance peaks as shown in Fig. 6.2b. It thus appears that both bias and gate voltage can be used to modulate the

conductance, and a conductance spectrum where both are varied simultaneously is given in the inset to Fig. 6.2b. Diamond-shaped regions are visible where the conductance is suppressed. Traces such as those in Fig. 6.2a are cross sections of this conductance spectrum at fixed gate voltage, whereas those in Fig. 6.2b are cross sections at fixed bias voltage. Before fabrication of the two buckles the device conductance did not change with gate voltage. It is thus evident that the modulation is due to the fabricated island.

These characteristics demonstrate Coulomb blockade (i.e. single-electron tunneling) at room temperature [1]. Coulomb blockade as a function of bias and gate voltage occurs in diamond shaped regions (cf. inset to Fig. 6.2b). Within each diamond, the number of electrons is fixed and electrons are added one by one to the island upon increasing the gate voltage. The height of the diamonds reads the bias voltage V^+ necessary to add an electron to the island, which defines an addition energy $E_{add} = eV^+ = e^2/C + \Delta E$ [9], where C is the sum of all capacitances to the nanotube island and ΔE the energy difference between consecutive quantum energy levels. We find $E_{add} = 120$ meV, which is slightly larger than the largest value of 115 meV reported in previous planar RTSETs [4]. The Coulomb blockade model describes all the basic device characteristics shown in Fig. 6.2a and b. Note that E_{add} is much larger than the thermal energy k_BT (k_B is Boltzmann's constant and T is the absolute temperature) at room temperature which explains the room-temperature operation of our devices.

We now turn to the device characteristics at low temperature. Examining the data at 30 K (Fig. 6.2c – e) reveals features that were not observed at room temperature. First, the data show less scatter due to a reduction in sample noise at low temperatures. Second, the $dI/dV(V)$ traces show peaked features (indicated by the lines in Fig. 6.2c) that shift along the bias voltage axis when changing the gate voltage. We believe that these peaks are associated with energy levels of the island that become available for electronic transport, leading to an increase in current. The peaks can be followed as a function of both bias and gate voltage in the conductance spectrum (see dashed lines in Fig. 6.2d and e). The distance between these lines along the bias-voltage axis is equal to $2\Delta E$. We find $\Delta E = 38$ meV. From the linear dispersion relation of nanotubes one estimates $\Delta E = hv_F/4L$ for a tube of finite length L, when the degeneracy between the two sets of energy levels in nanotubes has been lifted. Here v_F is the Fermi velocity, and h is Planck's constant. With $v_F = 8 \times 10^5$ m/s [10], we obtain 34 meV for the 25 nm island which compares very well to the measured value. This confirms

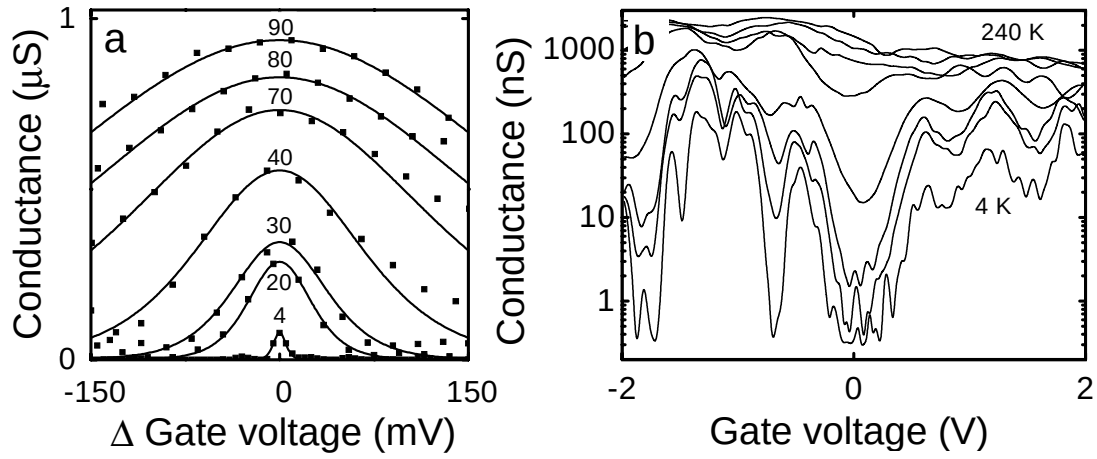

Figure 6.3: **a**) Zero-bias conductance versus gate voltage for a single conductance peak. Data are shown for T = 4, 20, 30, 40, 70, 80, and 90 K. The solid lines are fits to the function $G_{max}(T)/\cosh^2\left[2\left(\text{arccosh}\sqrt{2}\right)V_{gate}/w(T)\right]$ (see ref. [9]). The T dependence of the conductance maximum G_{max} and the full-width-at-half-maximum w is shown in Fig. 6.4. **b**) Multiple conductance peaks on a logarithmic scale for an extended range of gate voltage at T = 4, 40, 60, 70, 100, 170, 200, 220, and 240 K.

that the island behaves as a well-defined quantum box for the electrons. From the addition energy we can now extract the charging energy $E_C \equiv e^2/2C$, which reads 41 meV. It is unique to our devices that $\Delta E \sim E_C$, whereas in the ordinary case $E_C \gg \Delta E$. This is a direct result of the small size of these islands and the nature of the buckle junctions. In contrast to previous studies on straight undeformed nanotubes [10–13], the capacitances of the nanotube island to the nanotube leads (≈ 0.3 aF) are now a major contribution to the total capacitance C. Hence, while ΔE will increase with decreasing L, E_C will remain approximately constant, yielding a larger $\Delta E/E_C$ ratio.

Figure 6.3 shows the temperature dependence of the device conductance. A single conductance peak is plotted versus gate voltage in Fig. 6.3a. It is clear that *both* the conductance peak maximum G_{max} and the peak width w increase with increasing temperature. This is in striking contrast with what is expected for a conventional SET in both the classical ($k_BT > \Delta E$) and the quantum regime of Coulomb blockade ($k_BT < \Delta E$) : In both of the latter cases $w \propto T$, but G_{max} = constant or $G_{max} \propto 1/T$, respectively [9]. Note that our data also differ from previous results for carbon nanotube SET devices operating at low temperatures [10–14].

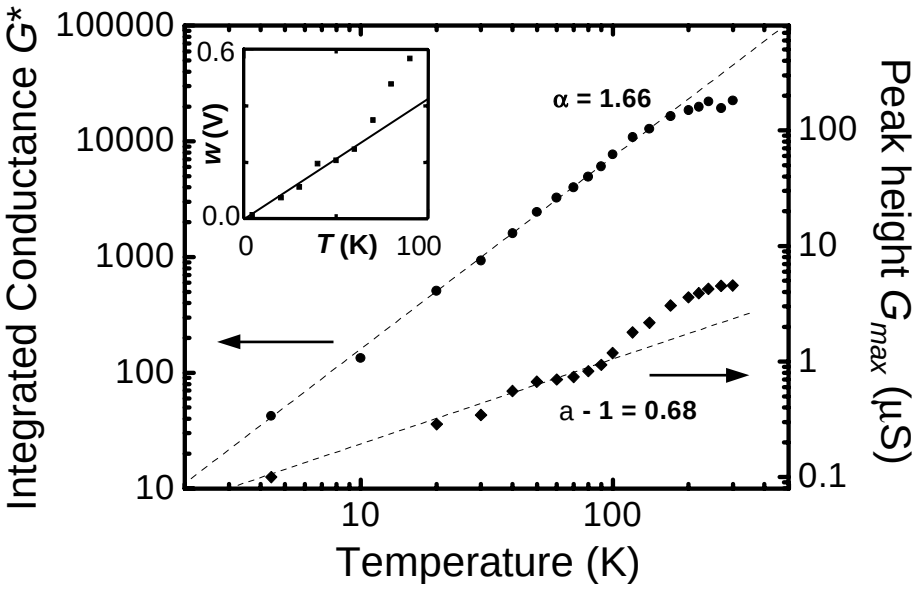

Figure 6.4: Power-law temperature dependence of the conductance, demonstrating correlated sequential tunneling through the nanotube SET device. Lower data (right-hand scale) shows the peak height $G_{max}(T)$ for the conductance peak in Fig. 6.3a, following a power-law function with exponent 0.68 (♦). The conductance integrated over the gate voltage range in Fig. 6.3b, $G^{\star}(T)$ (left-hand scale), also follows a power-law function with exponent 1.66 (•). Note the double-logarithmic scales. The inset shows the peak width w versus T which follows a linear behavior.

The conductance shows a power-law dependence on T as can be seen in Fig. 6.4, where $G_{max}(T)$ is plotted for the peak in Fig. 6.3a. From 4 to 90 K, it follows a power law $G_{max} \propto T^{0.68}$, while at higher temperatures it increases beyond this. The inset to Fig. 6.4 shows that w follows a linear temperature dependence $w \propto T$ at low temperatures, while it also deviates at higher temperatures. We can explain the high-temperature deviations from the overlap between adjacent peaks. Since the peak width increases with temperature, the peak tails start to overlap progressively with adjacent conductance peaks upon raising the temperature, leading to both a larger apparent peak height as well as a larger apparent width. We can correct for this by integrating the conductance over gate voltage, yielding an integrated conductance $G^{\star}$. We find a strong temperature dependence $G^{\star} \propto T^{1.66}$, in excellent agreement with the expected behavior $G^{\star} \propto T^{1+0.68}$ from $w(T)$ and $G_{max}(T)$. This power-law behavior persists well above the temperatures where both w and G_{max} deviate from the expected be-

havior, indicating that the deviations in measurements of w and G_{max} are indeed due to overlap of adjacent conductance peaks.

The power-law exponents observed in our experiments can *not* be explained by the available models. Recent transport experiments on metallic carbon nanotubes [8, 15–17] successfully employed a Luttinger-liquid model [18, 19] which derives from the one-dimensional electronic correlations in nanotubes. We therefore compare our experimental results to theoretical studies of a Luttinger island connected by tunnel barriers to two semi-infinite Luttinger liquids. So far, such studies have described transport in terms of sequential tunneling processes, with independent tunneling from the leads onto the island and from the island into the other lead [20–23]. This leads to $G_{max} \propto T^{\alpha_{end}-1}$ and $w \propto T$, where $\alpha_{end} = \frac{1}{4}(\frac{1}{g} - 1)$, with the Luttinger interaction parameter g characterizing the electron-electron interaction strength [18, 19]. Experiments [8, 15–17] show that g ranges between 0.19 and 0.26 in the case of carbon nanotubes, which leads to $G_{max} \propto T^{-0.2}$ and $G^{\star} \propto T^{0.8}$, in clear contradiction with the present data.

We therefore propose another mechanism, namely correlated sequential tunneling through the island. Here electrons tunnel coherently from the end of one nanotube lead to the end of the other nanotube lead through a quantum state in the island. In this picture, the island should be regarded as a single impurity [24]. This is reasonable, since the thermal length $L_T \equiv \hbar v_F / k_B T = 21$ nm at 300 K, and hence it is larger than the distance between the two barriers for all $T < 250$ K. The calculation for the conductance due to this tunneling mechanism is $G_{max} \propto T^{\alpha_{end-end}-1}$ and $G^{\star} \propto T^{\alpha_{end-end}}$, where $\alpha_{end-end} = 2\alpha_{end}$ [25]. Upon identifying $\alpha_{end-end}$ with the experimental value 1.66, we obtain $g = 0.23$, in excellent agreement with earlier values for nanotubes. This shows that the proposed mechanism is the relevant transport channel for the RTSET. The surprising dominance of correlated tunneling over sequential tunneling counters the common understanding for SETs and quantum dots [1]. Our model is further confirmed by data of the integrated differential conductance $(dI/dV)^{\star}$ versus bias voltage at large bias ($V > 10$ mV), which yields a power law $(dI/dV)^{\star} \propto V^{0.87}$ (not shown). One theoretically expects that the large bias voltage $eV \gg k_B T$ destroys the phase coherence necessary for correlated tunneling, and that conventional sequential tunneling will dominate [25]. The expected exponent for this process is $\alpha_{end} = \alpha_{end-end}/2 = 0.83$ which is again remarkably close to the value found experimentally.

For practical applications, a figure of merit of SETs is the input equivalent

charge noise q_n. Preliminary measurements on the present nanotube devices at 10 Hz and 60 K yielded $q_n \approx 2 \times 10^{-3}$ e/$\sqrt{\text{Hz}}$, which compares favorably to $q_n \approx 0.5 \times 10^{-3}$ e/$\sqrt{\text{Hz}}$ for conventional single-electron transistors which operate at mK temperatures [26]. The prototype nanotube RTSETs presented here were obtained by manipulation with an AFM. Future use in large-scale applications will require further developments in fabrication technology such as mechanical templates or chemical methods to create short nanotubes in a parallel process. RTSETs have some advantages over room-temperature field-effect transistors employing semiconducting nanotubes [27]. Because semiconducting nanotubes are, unlike metallic tubes, intrinsically prone to disorder and unintentional doping [28, 29], molecular-electronics components based on metallic tubes are preferred. The present work shows that short metallic nanotubes can be applied as RTSETs. It also exemplifies that the search for functional molecular devices often yields interesting fundamental science.

Acknowledgements

We thank R.E. Smalley and coworkers for prviding the carbon nanotube material, A. Bachtold, M.P.A. Fisher, L. Balents, P. Hadley, and Yu.V. Nazarov for discussions, and B. van den Enden for technical assistance. This work is supported by the Dutch Foundation for Fundamental Research on Matter (FOM) and the European Community SATURN project.

This chapter has been published in Science **293**, 76 (2001).

References

[1] H. Grabert and M. Devoret (eds) in *Single Charge Tunneling* (Plenum, New York, 1992).

[2] Y. Takahashi *et al.*, *Electron. Lett.* **31**, 136 (1995).

[3] K. Matsumoto *et al.*, *Appl. Phys. Lett.* **68**, 34 (1996).

[4] L. Zhuang, L. Guo, and S.Y. Chou, *Appl. Phys. Lett* **72**, 1205 (1998).

[5] C. Dekker, *Physics Today* **52 (5)**, 22 (1999).

[6] H.W.Ch. Postma, A. Sellmeijer, and C. Dekker, *Adv. Mater.* **17**, 1299 (2000).

[7] S. Iijima, C. Brabec, A. Maiti, and J. Bernholc, *J. Chem. Phys.* **104**, 2089 (1996).

[8] H.W.Ch. Postma, M. de Jonge, Z. Yao, and C. Dekker, *Phys. Rev. B* **62**, R10653 (2000).

[9] C.W.J. Beenakker, *Phys. Rev. B* **44**, 1646 (1991).

[10] S.J. Tans *et al.*, *Nature* **386**, 474 (1997).

[11] M. Bockrath *et al.*, *Science* **275**, 1922 (1997).

[12] D.H. Cobden, M. Bockrath, P.L. McEuen, A.G. Rinzler, and R.E. Smalley, *Phys. Rev. Lett.* **81**, 681 (1998).

[13] H.W.Ch. Postma, Z. Yao, and C. Dekker, *J. Low Temp. Phys.* **118**, 495 (2000).

[14] M. Bockrath *et al.*, *Science* **291**, 283 (2001).

[15] M. Bockrath *et al.*, *Nature* **397**, 598 (1999).

[16] Z. Yao, H.W.Ch. Postma, L. Balents, and C. Dekker, *Nature* **402**, 273 (1999).

[17] J. Nygard, D.H. Cobden, M. Bockrath, P.L. McEuen, and P.E. Lindelof, *Appl. Phys. A* **69**, 297 (1999).

[18] C.L. Kane, L. Balents, and M.P.A. Fisher, *Phys. Rev. Lett.* **79**, 5086 (1997).

[19] R. Egger and A.O. Gogolin, *Phys. Rev. Lett.* **79**, 5082 (1997).

[20] C.L. Kane and M.P.A. Fisher, *Phys. Rev. Lett.* **68**, 1220 (1992).

[21] A. Furusaki, *Phys. Rev. B.* **57**, 7141 (1998).

[22] A. Braggio, M. Grifoni, M. Sassetti, and F. Napoli, *Europhys. Lett.* **50**, 236 (2000).

[23] Although the first theoretical predictions for Luttinger liquid behavior already considered double-barrier devices, experimental evidence so far is scarce, see O. Auslaender *et al.*, *Phys. Rev. Lett.* **84**, 1764 (2000).

[24] M.P.A. Fisher and L. Balents, personal communication.

[25] M. Thorwart, M. Grifoni, H.W.Ch. Postma, and C. Dekker, *submitted to Phys. Rev. Lett,* (2001).

[26] A.B. Zorin *et al.*, *Phys. Rev. B* **53**, 13682 (1996).

[27] S.J. Tans, A.R.M. Verschueren, and C. Dekker, *Nature* **393**, 49 (1998).

[28] S.J. Tans and C. Dekker, *Nature* **404**, 834 (2000).

[29] A. Bachtold *et al.*, *Phys. Rev. Lett.* **84**, 6082 (2000).

Chapter 7

1/f noise in carbon nanotubes

H.W.Ch. Postma, T.F. Teepen, Z. Yao, and C. Dekker

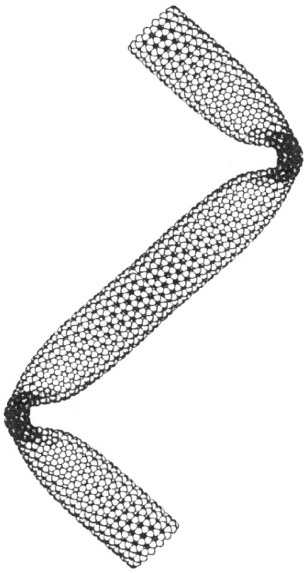

Abstract: The low-frequency electronic noise properties of individual single-wall metallic carbon nanotubes are investigated. The noise exhibits a $1/f$ frequency dependence and a V^2 voltage dependence. The noise power at 8 K appears to be three orders of magnitude smaller than at 300 K. As a demonstration of how these noise properties affect nanotube devices, a preliminary investigation of the noise characteristics of a fabricated intramolecular carbon nanotube single-electron transistor is presented.

The electronic properties of carbon nanotubes have attracted a lot of interest in both fundamental as well as application-driven studies [1]. All of these studies focussed on the DC electronic properties, and little is known about the AC or noise properties. Only recently, the noise characteristics of carbon nanotubes have become the subject of investigation. The first measurements show that the low-frequency electronic noise is dominated by $1/f$ noise [2, 3]. Many issues remain unclear however, for example, how the noise power depends on temperature. Knowledge of the noise characteristics is important to characterize performance of nanotube devices. The study of the fluctuation phenomena will also enable one to examine for instance correlation-induced reduced shot noise [4] in Luttinger liquids or bunching/anti-bunching-type phenomena that probe the quantum statistics [5, 6] of electrons in nanotubes. Here, we report a characterization of the low-frequency electronic noise properties of individual metallic single-wall carbon nanotubes. The frequency dependence follows Hooge's law. Upon lowering temperature to 8 K, the noise power is reduced by three orders of magnitude. As an example of how this low-frequency noise affects the performance of nanotube devices, we study the charge sensitivity of an intramolecular carbon-nanotube single-electron transistor.

Individual carbon nanotube samples are fabricated as described before [7]. Figure 7.1a shows an example of a straight nanotube, connected by metallic electrodes. On such samples we have characterized the amount of $1/f$ noise present in nanotubes. In Fig. 7.1b, a double-buckle nanotube is shown. We recently reported that these devices act as room-temperature single-electron transistors [8]. Here we present a first analysis of its noise properties and discuss the charge sensitivity of such devices.

The noise power spectral density has been measured for individual nanotubes as a function of the DC current I_{DC} at room temperature (Fig. 7.2). At $I_{DC} = 0$,

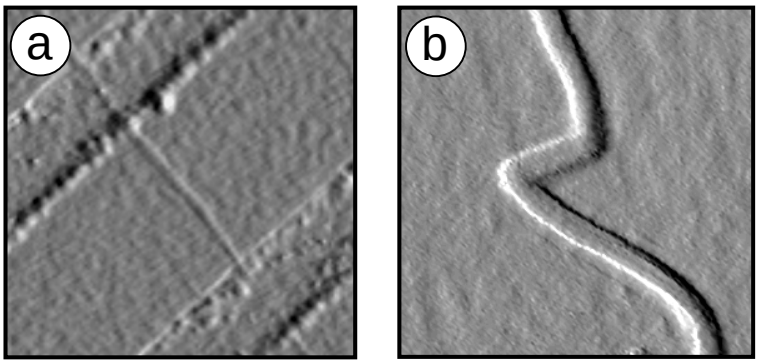

Figure 7.1: Atomic force microscope amplitude images of metallic carbon nanotubes. **a**) A straight nanotube connected by two Au electrodes lying on a SiO_2 surface. The image is 1 μm^2. **b**) A metallic nanotube with two buckles which have been induced with the atomic force microscope. The image size is 100×100 nm^2.

the voltage noise is white, i.e., it does not depend on frequency, and equals the expected value for thermal noise $4k_BTR = 2.1 \times 10^{-16}$ V^2/Hz of the nanotube, where $R = 12.6$ kΩ for this device. With increasing current, additional noise appears, which exhibits a $1/f$ frequency dependence. These two noise powers appear to add incoherently, i.e., $S_V = 4k_BTR + B/f$. The current dependence is studied in the inset to Fig. 7.2, where it is found that $B = AV_{DC}^2$. [9] The proportionality constant A thus found describes the full current and frequency dependence. All of these results are qualitatively consistent with the phenomenological dependence known as Hooge's law [10].

As postulated by Hooge, A depends on the number of charge carriers in the conductor N through $A = \gamma/N$, where $\gamma \approx 2 \times 10^{-3}$. [11] Although it is now understood that the γ value is not universal, it is a good starting point to compare the magnitude of noise in nanotubes to that in bulk conductors described by Hooge's law. The nanotubes described here contain about 2000 conduction electrons. [12] Using the magnitude of A found above, we find $\gamma_{nanotubes} \approx 4 \times 10^{-3}$. Earlier, Collins *et al.* found that this number was about 2 orders of magnitude larger. [2] Our material, however, shows much less noise and is in fact quite a low-noise conductor.

The temperature dependence of the $1/f$ noise is displayed in Fig. 7.3. With the current and frequency dependence given above, it suffices to display the value of A. It appears that the noise is reduced in a monotonous way by three orders of magnitude upon lowering the temperature. This has been measured in many

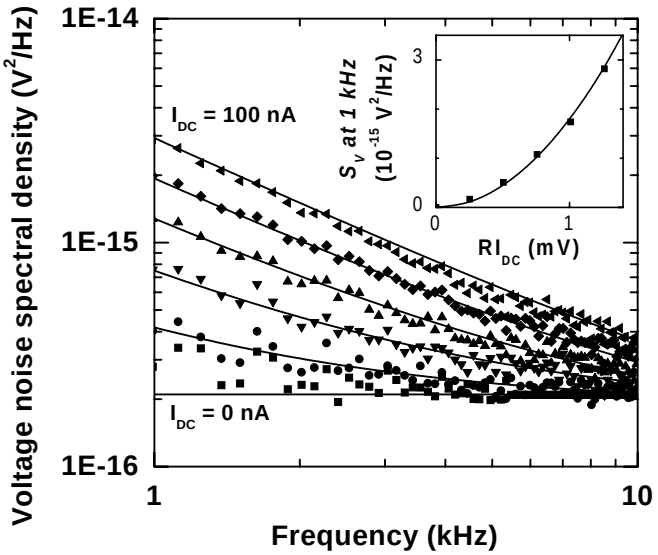

Figure 7.2: Noise spectra at $T = 300$ K for a nanotube with resistance $R = 12.6$ kΩ for various DC currents from 0 to 100 nA. The white noise visible at low I_{DC} is the expected thermal or Johnson-Nyquist noise of the sample $S_{V,JN} \equiv 4k_BTR = 2.1 \times 10^{-16}$ V^2/Hz, where k_B is Boltzmann's constant. The deviations from $1/f$ spectra at low current are due to $1/f$ noise from the amplifiers. The solid lines are fits with the function $S_V = S_{V,JN} + B/f$. The inset shows the excess $1/f$ noise at 1 kHz versus DC voltage $V_{DC} = RI_{DC}$. From the fit (solid line) we obtain $B = AV_{DC}^2 = 1.8 \times 10^{-6} V_{DC}^2$. The same value for A is found in voltage-biased measurements of the current noise $S_I = S_{I,JN} + AI_{DC}^2/f$, where $S_{I,JN} \equiv 4k_BT/R$.

individual nanotube samples that we have studied.

In the commonly employed model for $1/f$ noise, it is assumed that fluctuating two-level systems in the surrounding give rise to a fluctuating potential profile, which leads to this low-frequency noise [10]. Within this model it is reasonable that a reduction of the temperature will lead to reduction of the noise, since at lower temperatures these two-level systems will freeze into local energy minima. The chemical stability, high degree of regularity and detailed knowledge of the electronic and mechanical structure of carbon nanotubes provide the right ingredients to study the origin of $1/f$ noise in detail. This, however, is beyond the scope of this brief chapter.

As an example of how the low-frequency noise affects the performance of a nanotube device, we have studied the noise properties of the double-buckle sample in Fig. 7.1b. In these samples, the addition of a single electron to the

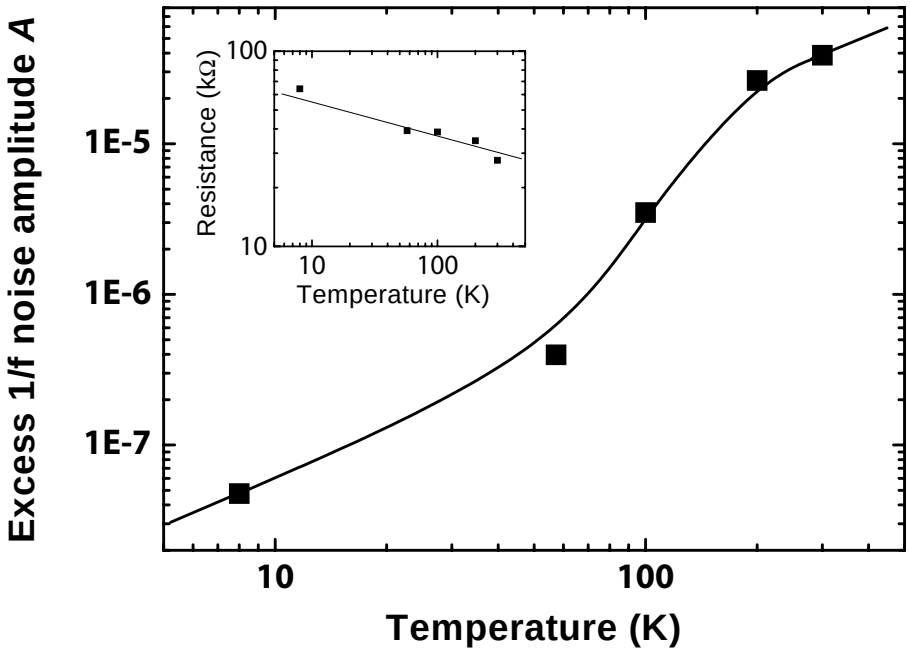

Figure 7.3: Excess $1/f$ noise power versus temperature for a single carbon nanotube. Plotted is the proportionality constant A of the $1/f$ noise spectral density $S_V = AV_{DC}^2/f$ as obtained from an analysis of the voltage and frequency dependence as is shown in Fig. 7.2. The inset shows the temperature dependence of the resistance of the nanotube. The lines are guides to the eye.

island between the two buckles costs a large energy due to the Coulomb charging of the island [14]. When the thermal energy k_BT is smaller than this charging energy, current is blocked. The blockade can be lifted, however, by increasing the electrostatic potential of the nanotube by means of a conducting nearby gate. Current can then flow. If the gate voltage is increased further, however, current is again blocked. This leads to a series of current peaks as a function of gate voltage, see Fig. 7.4a. The noise at 10 Hz has been measured versus gate voltage. Again peaked features are observed, see Fig. 7.4b. To characterize the performance of such a single-electron transistor, one determines how accurately charge on the gate can be measured. Thus, the measured current noise $\sqrt{S_I}$ is divided by the gate voltage sensitivity (dI/dV_g), and multiplied by the gate capacitance to obtain the so-called input equivalent charge noise $q_{noise} = C_g\sqrt{S_I}/(dI/dV_g)$, which is being displayed in Fig. 7.4c. [15] It diverges periodically (with a period twice as small as the distance between current peaks), every time the gate voltage sensitivity vanishes. In between, it reaches its optimum value of $2\times10^{-3}e/\sqrt{\text{Hz}}$ at

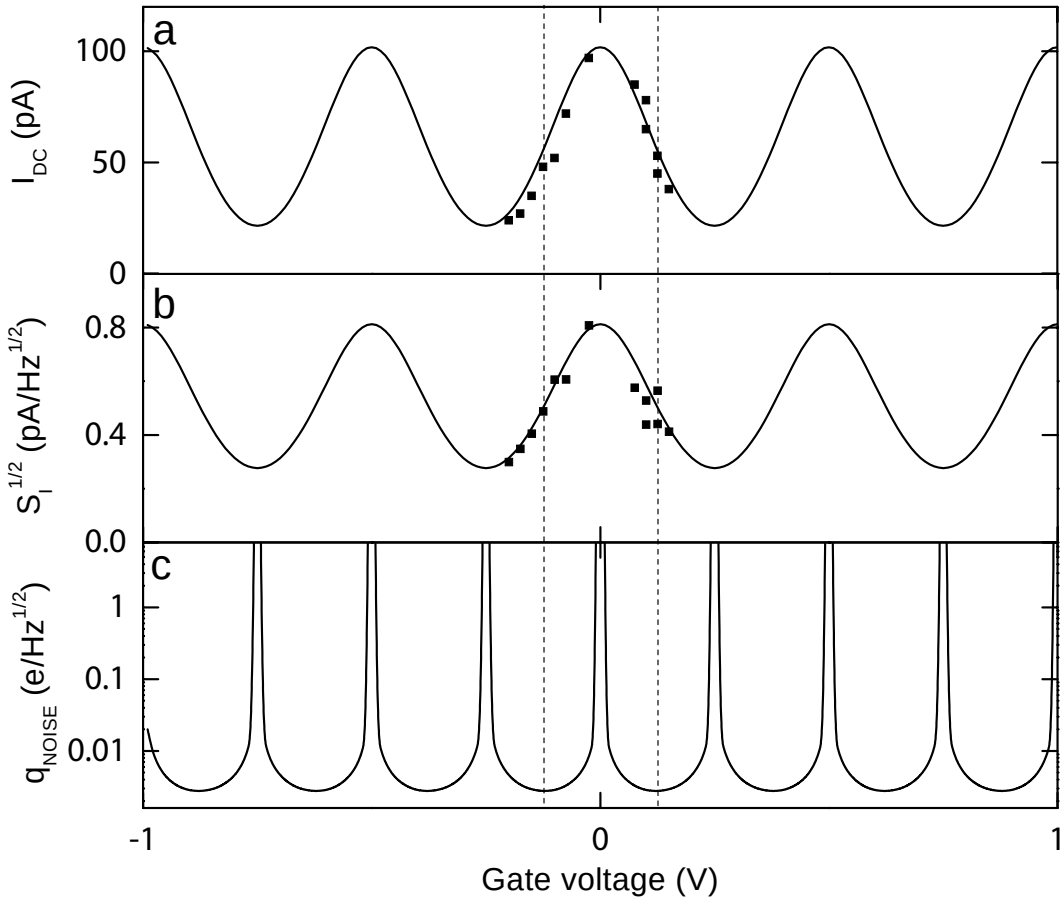

Figure 7.4: Noise characteristics of the carbon nanotube single-electron transistor shown in Fig. 7.1b at 60 K and 10 Hz. Both current and current noise depend on the gate voltage as is visible in (a) and (b). Both are fit (solid lines) with a superposition of Coulomb conductance peaks [13]. In (c), the results of these fits are used to determine the input equivalent charge noise of the device.

the gate voltage indicated by the vertical dashed lines. This compares favorably to values $q_{noise} \approx 0.5 \times 10^{-3}$ e/$\sqrt{\text{Hz}}$ for conventional single-electron transistors which operate at mK temperatures [16], because the data on the nanotube device are obtained at 60 K and the noise is reduced considerably as a function of temperature (see above).

We conclude with an estimate of the measurement bandwidth needed to observe shot noise $S_I = 2eI_{DC}$, which is a good approximation of the bandwidth needed to observe reduced shot noise or bunching/anti-bunching type effects. For this estimate we – optimistically – assume that samples may be fabricated with a 10 kΩ resistance and a $1/f$ noise power amplitude $A \approx 10^{-8}$ and we focus on the

properties at 4 K. For simplicity we assume that all the amplifier noise can be reduced sufficiently such that only the thermal noise of the sample (2.2×10^{-26} A^2/Hz) dominates at low current. The total noise may then be written as

$$S_I = 4k_BT/R + 2eI_{DC} + AI_{DC}^2/f \qquad .$$

For the observation of shot noise, we obviously require that $\eta = (4k_BT/R + AI_{DC}^2/f)/2eI_{DC} < 1$, from which we deduce two boundary conditions for $I_- < I_{DC} < I_+$. At low current $I_{DC} < I_- \approx 4k_BT/\eta 2eR$, the thermal noise dominates, whereas at high current $I_{DC} > I_+ \approx 2ef\eta/A$ the $1/f$ noise dominates. Finally we require that $I_+ \gg I_-$ since one needs to observe the current dependence of the shot noise. If an experimental uncertainty of 10 % is sufficient ($\eta = 1/10$) and $I_+/I_- = 10$, we find $f > 2.2$ MHz. This frequency range is not accessible with our current setup, but is certainly accessible with a dedicated setup.

Acknowledgments

We thank R.E. Smalley and coworkers for the carbon nanotube material, A. Morpurgo for discussions, and B. van den Enden and R. Schouten for technical assistance. This work is supported by the Dutch Foundation for Fundamental Research on Matter (FOM) and the European Community SATURN project. The image on page 73 has been adapted from [17].

This chapter will appear in 'XXXV Moriond Les Arcs Conference Proceedings, Edition Frontiers, France, 2001'

References

[1] C. Dekker, *Physics Today* **52 (5)**, 22 (1999).

[2] P.G. Collins, M.S. Fuhrer, and A. Zettl, *Appl. Phys. Lett.* **76**, 894 (2000).

[3] L. Roschier, R. Tarkiainen, M. Ahlskog, M. Paalanen, and P. Hakonen, *Appl. Phys. Lett* **78**, 3295 (2001).

[4] R. De-Picciotto *et al.*, *Nature* **389**, 162 (1997).

[5] M. Henny *et al.*, *Science* **284**, 296 (1999).

[6] W.D. Oliver, J. Kim, R.C. Liu, and Y. Yamamoto, *Science* **284**, 299 (1999).

[7] Z. Yao, H.W.Ch. Postma, L. Balents, and C. Dekker, *Nature* **402**, 273 (1999).

[8] H.W.Ch. Postma, T.F. Teepen, Z. Yao, M. Grifoni, and C. Dekker, *Science* **293**, 76 (2001).

[9] It is often convenient to assume that $S_{V,1/f} \propto V^2/f$ or $S_{I,1/f} \propto I^2/f$. In general, however, it is found that $S_{1/f} \propto V^{2+\alpha}/f^{1+\beta}$, where $|\alpha| \ll 1, |\beta| \ll 1$ are material dependent numbers. Here, we assume $\alpha = \beta = 0$.

[10] P. Dutta and P.M. Horn, *Rev. Mod. Phys.* **53**, 497 (1981).

[11] F.N. Hooge, *Phys. Lett. A* **29**, 139 (1969).

[12] This estimate is for this nanotube with a length of 500 nm. We did not perform a systematic study of the $1/N$ dependence.

[13] C.W.J. Beenakker, *Phys. Rev. B* **44**, 1646 (1991).

[14] H. Grabert and M. Devoret (eds) in *Single Charge Tunneling* (Plenum, New York, 1992).

[15] Please note that while $eV_{DC} \ll k_BT$, both the current noise and the DC current depend on bias voltage through the relations $I_{DC} \propto V_{DC}$ and $\sqrt{S_I} \propto V_{DC}$, so the bias voltage dependence of q_{noise} cancels.

[16] A.B. Zorin *et al.*, *Phys. Rev. B* **53**, 13682 (1996).

[17] S. Iijima, C. Brabec, A. Maiti, and J. Bernholc, *J. Chem. Phys.* **104**, 2089 (1996).

Summary

This thesis presents the results of electron-transport experiments performed on individual single-wall carbon nanotubes. Carbon nanotubes are molecules entirely made of carbon atoms. Owing to their special shape, they are extremely stiff but also very flexible. The electronic properties are determined by the exact symmetry of the nanotube lattice, resulting in either metallic or semiconducting behavior. Due to their small diameter, electronic motion is directed in the length direction of the nanotube, making them ideal systems to study e.g. one-dimensional transport phenomena (Ch. 1).

First, we present mK-temperature non-linear current-voltage characteristics of an individual single-wall carbon nanotube as a function of magnetic field (Ch. 2). The measurements show Coulomb blockade and resonant tunneling through single molecular levels. Correlations between the addition spectrum and the excitation spectrum are observed and the magnetic field dependence of the addition and excitation spectra is discussed.

Then, we report electrical transport measurements on carbon nanotubes with naturally occurring intramolecular junctions (Ch. 3). We find that a metal-semiconductor junction behaves like a rectifying diode with nonlinear transport characteristics that are strongly asymmetric with respect to bias polarity. In the case of a metal-metal junction, the conductance appears to be strongly suppressed and it displays a power-law dependence on temperatures and applied voltage, consistent with tunnelling between the ends of two Luttinger liquids.

In order to further study carbon nanotube intramolecular junctions, we developed an atomic force microscope (AFM) manipulation technique (Ch. 4). The tip of the AFM can be used to create carbon nanotube junctions by changing the position and shape of individual single-wall carbon nanotubes on a SiO_2 surface. With this manipulation technique, we are able to bend, buckle, cross, and break nanotubes, and to unravel a nanotube 'crop circle' into a single tube. Tapping-mode AFM measurements of the height of a carbon nanotube on the surface always yield values smaller than the nanotube diameter. Variation of the scan parameters shows that this is due to a tapping deformation by the tip. The tapping deformation of manipulated nanotube crossings and buckles is discussed as well.

Using this manipulation technique, we have created nanotube junctions such

as buckles and crossings within metallic carbon nanotubes connected to electrodes (Ch. 5). The electronic transport properties of these manipulated structures show that they form electronic tunnel junctions. The conductance shows power-law behavior as a function of bias voltage and temperature, which can be well modeled by a Luttinger liquid model for tunneling between two nanotube segments separated by the manipulated junction.

Room-temperature single-electron transistors can be realized within individual metallic single-wall carbon nanotube molecules as shown in Ch. 6. The devices feature a short (down to 20 nm) nanotube section that is created by inducing local barriers into the tube using the AFM. Coulomb charging is observed at room temperature, with an addition energy of 120 meV which significantly exceeds the thermal energy. At low temperatures, we resolve the quantum energy levels corresponding to the small island. We observe unconventional power-law dependencies in the measured transport properties for which we develop a resonant-tunneling Luttinger-liquid model.

The low-frequency electronic noise properties of individual single-wall metallic carbon nanotubes are investigated in Ch. 7. The noise exhibits a $1/f$ frequency dependence and a V^2 voltage dependence. The noise power at 8 K appears to be three orders of magnitude smaller than at 300 K. As a demonstration of how these noise properties affect nanotube devices, a preliminary investigation of the noise characteristics of a fabricated intramolecular carbon nanotube single-electron transistor is presented.

Henk Postma
Delft, October 2001

Samenvatting

In dit proefschrift beschrijven we resultaten van experimenten die zijn uitgevoerd op individuele enkelwandige koolstof nanobuizen. Koolstof nanobuizen zijn moleculen die slechts bestaan uit koolstofatomen. Dankzij de speciale vorm die zij hebben, zijn ze zowel heel sterk als ook flexibel. De elektrische geleidingseigenschappen worden bepaald door de exacte symmetrie van het nanobuis rooster, waardoor ze of een metallische danwel een halfgeleidende eigenschap kunnen hebben. Omdat ze een zeer kleine diameter hebben, verplaatsen de elektronen zich in de lengterichting van de nanobuis. Daarom zijn koolstof nanobuizen een modelsysteem om ééndimensionale geleidingseigenschappen te onderzoeken (Hfst. 1).

Om te beginnen tonen we niet-lineaire stroom-spannings karakteristieken van een individueel enkelwandige koolstof nanobuis verkregen op mK temperatuur als functie van het magneetveld (Hfst. 2). De resultaten laten Coulomb blokkade zien en resonant tunnelen door individuele moleculaire toestanden. We ontdekken correlaties tussen het additie- en het excitatiespectrum en we beschrijven de magneetveldafhankelijkheid van de additie- en excitatiespectra.

Hierna beschrijven we elektrische transportmetingen aan koolstof nanobuizen met toevallig aanwezige intramoleculaire verbindingen (Hfst. 3). We ontdekken dat een metaal-halfgeleider verbinding zich gedraagt als een gelijkrichtende diode met niet-lineaire transportkarakteristieken met een zeer asymmetrische spanningsafhankelijkheid. Bij een metaal-metaal overgang vinden we dat de geleiding sterk onderdrukt is en als een machtswet afhangt van de temperatuur en aangelegde spanning, consistent met tunnelen tussen de einden van twee Luttinger vloeistoffen.

Om koolstof nanobuis intramoleculaire juncties verder te bestuderen, hebben we een manipulatietechniek ontwikkeld op basis van de atomaire kracht microscoop (AFM) (Hfst. 4). Door met de punt van de AFM de plaats en vorm van individuele enkelwandige nanobuizen op een SiO_2 oppervlak te veranderen, kunnen we koolstof nanobuis juncties maken. We laten zien hoe we op deze manier nanobuizen kunnen buigen, knikken, kruisen en breken. Ook tonen we hoe we een koolstof nanobuis cirkel ontrafelen tot een enkele nanobuis. Bij het in beeld brengen van koolstof nanobuizen op een oppervlak met de AFM in de zgn. *tapping-mode* lijken de buizen altijd lager dan de diameter van de nanobuis. Door

de instellingen van de AFM te veranderen laten we zien dat dit komt doordat we de nanobuis met de punt van de AFM indrukken. Hetzelfde effect treedt ook op bij nanobuis kruisingen en knikken.

Met deze manipulatietechniek hebben we kruisingen en knikken gemaakt in koolstof nanobuizen die met meetelektroden verbonden zijn (Hfst. 5). De elektrische geleidingseigenschappen van deze juncties laten zien dat ze elektrische tunneljuncties vormen. De geleiding hangt als een machtswet af van de temperatuur en de aangelegde spanning, hetgeen goed beschreven wordt door een Luttinger vloeistof model voor het tunnelen tussen de twee segmenten aan weerszijden van de junctie.

Enkel elektron transistoren die werken bij kampertemperatuur zijn gemaakt in individuele enkelwandige metallische koolstof nanobuizen, zoals we laten zien in Hfst. 6. Deze transistoren bevatten een kort nanobuis segment (vanaf 20 nm) dat is gemaakt door met de AFM plaatselijke barrières te induceren. We zien Coulomb ladingsgedrag op kamertemperatuur met een additie-energie van 120 meV, hetgeen significant hoger is dan de thermische energie. Op lage temperaturen zien we de quantum energieniveaus van het kleine eiland. Ook zien we dat de geleidingseigenschappen onconventionele machtswetten volgen. Om dit te beschrijven ontwikkelen we een resonant tunnelmodel op basis van de Luttinger vloeistof theorie.

In Hfst. 7 bestuderen we de laagfrequente elektronische ruiseigenschappen van individuele enkelwandige metallische koolstof nanobuizen. Deze ruis vertoont een $1/f$ frequentie- en een V^2 spanningsafhankelijkheid. Het ruisvermogen is op een temperatuur van 8 K drie ordegrootten kleiner dan op 300 K. We laten een analyse van de ruiseigenschappen van een intramoleculaire koolstof nanobuis enkel elektron transistor zien als een voorbeeld van de invloed van deze ruiseigenschappen op de prestatie van componenten op basis van koolstof nanobuizen.

Henk Postma
Delft, oktober 2001

Curriculum vitæ

Hendrik W. Ch. Postma

Dec 30, 1973	Born in Brielle, The Netherlands
1986 – 1992	Gymnasium at Christelijk Gymnasium Sorghvliet, The Hague
1992 – 1997	M.Sc. in Physics at Leiden University, graduate research in 'Quantum Fluids III' group of Prof.dr. G. Frossati subject : elastic and magnetic properties of alloys for resonant detection of gravitational waves
1997 – 2001	Ph.D. research at Delft University of Technology in 'Quantum Transport' group of Prof.dr.ir. J.E. Mooij, and 'Molecular Biophysics' group of Prof.dr. C. Dekker subject : carbon nanotube junctions and devices
2002 –	Postdoctoral fellow at California Institute of Technology in the group of Prof.dr. M.L. Roukes

List of publications

1. *1/f noise in carbon nanotubes*
   H.W.Ch. Postma, T.F. Teepen, Z. Yao, and C. Dekker
   To appear in *XXXV Moriond Les Arcs Conference Proceedings, Edition Frontiers, France, 2001*

2. *Correlated resonant tunneling in intramolecular carbon nanotube quantum dots*
   M. Thorwart, M. Grifoni, H.W.Ch. Postma, and C. Dekker
   submitted to Phys. Rev. Lett, (2001)

3. *Carbon nanotube single-electron transistors at room temperature*
   H.W.Ch. Postma, T.F. Teepen, Z. Yao, M. Grifoni, and C. Dekker
   Science **293**, 76–79 (2001)

4. *Single-electron effects in metals and nanotubes for nanoscale circuits*
   P. Hadley, C.P. Heij, G. Lientschnig, T.F. Teepen, H.W.Ch. Postma, and C. Dekker
   Proceedings of the MIOP (2001)

5. *Electrical transport through carbon nanotube junctions created by mechanical manipulation*
   H.W.Ch. Postma, M. de Jonge, Z. Yao, and C. Dekker
   Phys. Rev. B **62**, R10653–R10656 (2000)

6. *Manipulation and imaging of individual single-walled carbon nanotubes with an atomic force microscope*
   H.W.Ch. Postma, A. Sellmeijer, and C. Dekker
   Adv. Mater. **17**, 1299–1302 (2000)

7. *Electron addition and excitation spectra of an individual single-wall carbon nanotube molecule*
   H.W.Ch. Postma, Z. Yao, and C. Dekker
   J. Low Temp. Phys. **118**, 495–507 (2000)

8. *Carbon nanotube intramolecular junctions*
   Z. Yao, H.W.Ch. Postma, L. Balents, and C. Dekker
   Nature **402**, 273–276 (1999)